# ESAT-6 undergoes self-association at phagosomal pH and an ESAT-6 specific nanobody restricts M. tuberculosis growth in macrophages

Timothy A Bates[1], Mila Trank-Greene[1], Xammy Nguyenla[1], Aidan Anastas[1], Ilaria R Merutka[1], Shandee D Dixon[1], Anthony Shumate[2], Abigail R Groncki[1], Matthew AH Parson[3], Eric Barklis[1], John E Burke[3,4], Ujwal Shinde[2], Hidde L Ploegh[5], Fikadu G Tafesse[1,6]

[1]Department of Molecular Microbiology and Immunology, Oregon Health & Sciences University, Portland, Oregon, United States.

[2]Department of Chemical Physiology and Biochemistry, Oregon Health & Science University, Portland, Oregon, United States.

[3]Department of Biochemistry and Microbiology, University of Victoria, Victoria, Canada.

[4]Department of Biochemistry and Molecular Biology, The University of British Columbia, Vancouver, Canada.

[5]Program in Cellular and Molecular Medicine, Boston Children's Hospital, Harvard Medical School, Boston, Massachusetts, United States.

[6]Correspondence to tafesse@ohsu.edu

## Abstract

*Mycobacterium tuberculosis* (Mtb) is known to survive within macrophages by compromising the integrity of the phagosomal compartment in which it resides. This activity primarily relies on the ESX-1 secretion system, predominantly involving the protein duo ESAT-6 and CFP-10. CFP-10 likely acts as a chaperone, while ESAT-6 likely disrupts phagosomal

membrane stability via a largely unknown mechanism. we employ a series of biochemical analyses, protein modeling techniques, and a novel ESAT-6-specific nanobody to gain insight into the ESAT-6's mode of action. First, we measure the binding kinetics of the tight 1:1 complex formed by ESAT-6 and CFP-10 at neutral pH. Subsequently, we demonstrate a rapid self-association of ESAT-6 into large complexes under acidic conditions, leading to the identification of a stable tetrameric ESAT-6 species. Using molecular dynamics simulations, we pinpoint the most probable interaction interface. Furthermore, we show that cytoplasmic expression of an anti-ESAT-6 nanobody blocks Mtb replication, thereby underlining the pivotal role of ESAT-6 in intracellular survival. Together, these data suggest that ESAT-6 acts by a pH dependent mechanism to establish two-way communication between the cytoplasm and the Mtb-containing phagosome.

## Introduction

Tuberculosis (TB), caused by *Mycobacterium tuberculosis* (Mtb), is a major global health concern, claiming over 1.6 million lives annually. Mtb is highly adept at evading the immune system, and it can persist within an infected person for decades. This situation is worsened by the nearly 1.7 billion people globally who harbor a dormant Mtb infection (Houben and Dodd, 2016), coupled with the rising trend of drug-resistant TB cases (World Health Organization, 2022).

To successfully establish an infection in the host, Mtb utilizes a plethora of virulence factors delivered via its several ESX-secretion systems. Studies have indicated that Mtb has the ability to damage the phagosomal membrane, a process that is heavily reliant on the activity of the ESX-1 secretion system (Conrad et al., 2017; López-Jiménez et al., 2018; Schnettger et al., 2017). Currently, the most probable candidate driving ESX-1 dependent lytic activity is the well-known T cell antigen, the 6 kDa early secreted antigenic target (ESAT-6, or EsxA) ) (Andersen et al., 1995; Sørensen et al., 1995), after which the ESX family of T7SSs was originally named (Gey van Pittius

46 et al., 2001). Secretion of the various ESX-1 substrates are known to be highly complex and
47 interdependent, and while the full scope of ESX-1 components and substrates is still being worked
48 out, many individual ESX-1 component knockouts are known to phenocopy the ESAT-6 deletion,
49 indicating that ESAT-6 itself is responsible for the lion's share of the activity (Chen et al., 2012;
50 Clemmensen et al., 2017; Cronin et al., 2022; Lienard et al., 2020; Sanchez et al., 2020).

51 Over the last few decades, there have been numerous studies focused on uncovering the
52 possible mechanism of membrane lysis by ESAT-6 (Augenstreich et al., 2020; Conrad et al., 2017;
53 de Jonge et al., 2007; Kinhikar et al., 2010; Koo et al., 2008; Lienard et al., 2020; Osman et al.,
54 2022), and how this might lead to escape of Mtb from the phagosome (Houben et al., 2012).
55 However, the field has been plagued by setbacks such as the discovery that many studies prior
56 to 2017 showing membrane disruption by ESAT-6 were confounded by the contamination with the
57 detergent ASB-14, which was originally added to remove endotoxin (Conrad et al., 2017).
58 Consequently, most recent studies have focused on the use of intact bacteria in assays, frequently
59 with the closely related *Mycobacterium marinum* (Mm), to avoid using recombinant proteins. The
60 conclusions of these experiments are complicated by the interdependent nature of ESX-1
61 structural components, chaperones, and substrates (Augenstreich et al., 2020; Osman et al.,
62 2022; Santucci et al., 2022). Mm has been a valuable model for working out ESX-1 and ESAT-6
63 function, and many of the key studies in the field have used Mm exclusively. However, the unique
64 characteristics of Mm compared to Mtb can sometimes leads to differing results, and conclusions
65 drawn from one species do not always apply to the other (Bosserman et al., 2019; Carlsson et
66 al., 2009; Lienard et al., 2020; Osman et al., 2022; Smith et al., 2008). This is important because
67 the membranolytic activity of the ESX-1 seems to be highly context dependent, and more
68 biochemical work is needed to work out the specific contributions of ESAT-6 to the membrane
69 disruption phenotype.

70 Despite extensive research, the precise mechanism of ESAT-6 action remains elusive.
71 This study aims to bridge this gap by performing comprehensive biochemical and cellular
72 investigations of ESAT-6 under neutral and acidic conditions. We use biolayer interferometry (BLI)
73 to measure the tight association between ESAT-6 and CFP-10, and the pH dependent ESAT-6
74 self-association. We use fluorescence microscopy to directly observe formation of large ESAT-6
75 complexes, and we measure the stoichiometry of ESAT-6 under different pH conditions using
76 multi-angle light scattering. We then use molecular dynamics-based modeling to evaluate the
77 most likely modes of ESAT-6 interaction. We also generated a novel ESAT-6-binding alpaca-
78 derived nanobody, E11rv, to further define the significance of ESAT-6 during Mtb infection. We
79 perform biochemical characterization of E11rv, as well as functional testing, which showed
80 inhibition of Mtb growth inside macrophages treated with E11rv or expressing cytoplasmic E11rv.

# 81 Results

## 82 Recombinant ESAT-6 and CFP-10 purification

83 In seeking to perform functional studies of ESAT-6 and CFP-10, we produced recombinant
84 protein using *E. coli* expression plasmids available from BEI Resources: pMRLB.7 (NR-50170)
85 containing ESAT-6, and pMRLB.46 (NR-13297) containing CFP-10. Both of these plasmids have
86 been used extensively in literature, including many of the most influential biochemical
87 characterization studies (Augenstreich et al., 2020; Behura et al., 2019; Chen et al., 2019; Choi
88 et al., 2010; Conrad et al., 2017; de Jonge et al., 2007; Eitson et al., 2012; Gallegos et al., 2008;
89 Harrison et al., 2014; Koyuncu et al., 2021; Lim et al., 2016; Mukherjee et al., 2007; Niazi et al.,
90 2015; Osman et al., 2022; Pathak et al., 2007; Peng et al., 2011; Refai et al., 2015; Smith et al.,
91 2008; Stavri et al., 2012; Vesosky et al., 2010; Woolhiser et al., 2007; Xiao et al., 2016; Yang et
92 al., 2008). The specification sheet for pMRLB.7 indicates that it includes a C-terminal FALE
93 solubility tag and subsequent Histidine affinity tag while pMRLB.46 indicates that it contains only

94 a C-terminal Histidine tag. We performed sequencing of both plasmids (Figs 1A and S1), and
95 noticed a stretch of 10 additional amino acids ahead of the reported tags in the pMRLB.7 plasmid.
96 The precise amino acid sequence of the pMRLB.46 plasmid has not been reported, but it appears
97 to contain 4 additional amino acids ahead of the expected tag. Importantly, we were able to
98 confirm that the full and complete sequences of ESAT-6 and CFP-10 are each contained in their
99 respective plasmids, and the inconsistencies fall within the C-terminal tag regions of each protein
100 (Figs 1A and S1).

101 Expression and purification by Nickel-NTA chromatography resulted in bands of the
102 expected sizes by SDS-PAGE and $His_6$-specific western blot (Fig 1B). Amino acid sequences of
103 the recombinant proteins were also confirmed by mass spectrometry (MS), where it was observed
104 that CFP-10 undergoes N-terminal methionine excision in our *E. coli* expression system (Fig S2)
105 (Giglione et al., 2004; Hirel et al., 1989). Size exclusion chromatography (SEC) showed
106 appropriate relative retention volumes and combining equimolar quantities of ESAT-6 with CFP-
107 10 resulted in a leftward shift, suggesting correct dimerization (Fig 1C).

## 108 Dimerization of ESAT-6 and CFP-10 at neutral pH

109 To validate that ESAT-6 and CFP-10 are forming a native dimer, we next performed native-
110 PAGE with different ratios of the two proteins (Fig 2A). We incubated ESAT-6 and CFP-10 for 1
111 hour at 4°C prior to running the gels, combining them in different ratios. The isoelectric point of
112 ESAT-6 and CFP-10 are both quite low, for our constructs they are 5.18 (net charge -8.22 at pH
113 7.4) and 5.72 (net charge -5.27 at pH 7.4), respectively. Thus, we oriented the positive electrode
114 toward the bottom of the gel. As expected, we observed that ESAT-6 ran faster than CFP-10.
115 Combinations of each showed a distinct third band of intermediate charge which was greatest in
116 the 1:1 mixture and absent in each pure protein, indicating formation of a 1:1 complex with no
117 intermediate species. This aligns with our results from Fig 1C, and aligns with historical research

118 on the interaction between ESAT-6 and CFP-10 (Poulsen et al., 2014; Renshaw et al., 2005,
119 2002).

120 Another commonly used test of ESAT-6 function is hemolysis, or the ability to damage red
121 blood cell (RBC) membranes and release hemoglobin. Historical studies reported that ESAT-6
122 was able to cause hemolysis, but Conrad et al. discovered that most of this hemolytic activity was
123 due to detergent contamination with ASB-14, which is commonly added during the wash steps of
124 Nickel-NTA purification to remove endotoxin (Conrad et al., 2017). Our recombinant ESAT-6 was
125 produced without detergent, and we confirmed that it was not able to induce hemolysis at any pH
126 between 4.5 and 7.5 (Fig S3). However, the hemolysis assay still finds contemporary use when
127 testing the ability of whole bacteria to induce membrane damage in an ESX-1 and contact-
128 dependent manner (Augenstreich et al., 2020; Bosserman et al., 2019; Conrad et al., 2017;
129 Osman et al., 2022). In such experiments, RBCs are mixed with log-phase bacterial cultures at
130 high MOI and pelleted by centrifugation to force direct contact. Similar to previous reports, we
131 found that *Mycobacterium marinum* (Mm) is capable of efficiently causing hemolysis within 2
132 hours (Fig 2B). In contrast, we found that Mtb was incapable of hemolysis over a similar time
133 frame. It is well established that Mm-induced hemolysis is ESX-1 dependent, but our results
134 suggest that Mtb must lack one or more factors necessary for efficient hemolysis. One previous
135 study was able to induce hemolysis using Mtb, but this required 48 hours instead of the typical 2
136 (Augenstreich et al., 2020).

## 137 Binding kinetics of ESAT-6 and CFP-10

138 To measure the binding strength of ESAT-6 and CFP-10 we developed a biolayer
139 interferometry (BLI) assay to measure their interactions (Fig 3A). We first measured the ability of
140 ESAT-6 and CFP-10 to form homo-oligomers or hetero-oligomers (Fig 3B), and found that they
141 preferentially formed hetero-oligomers. ESAT-6 showed a small, but measurable amount of self-
142 association, while CFP-10 showed no self-association. The dissociation constant ($K_D$) of the

143 ESAT-6/CFP-10 heterodimer has not hitherto been directly measured, but Renshaw et al.
144 estimated an upper bound of 10nM (Renshaw et al., 2002). We performed a detailed
145 measurement of the ESAT-6/CFP-10 association and measured a $K_D$ of 220 pM, indicating
146 exceptionally tight binding (Fig 3C). ESAT-6 self-association resulted in reduced overall binding
147 to the sensor and displayed a rapid on rate, but also a rapid off rate (Fig 3D). The curve shape is
148 suggestive of something other than traditional 1:1 binding, but for comparison purposes we
149 calculated an apparent $K_D$ of approximately 1.5 μM, weaker than that of the ESAT-6/CFP-10
150 association.

151 Because Mtb often exists in an acidified compartment, we tested whether ESAT-6 binding
152 changes under low pH conditions, the likes of which may be found in macrophage phagosomes
153 (Canton et al., 2014). Surprisingly, ESAT-6 displayed robust self-association at pH 4.5 (Fig 3E),
154 resulting in several-fold more mass attaching to the sensor than even the ESAT-6/CFP-10
155 association at neutral pH. The apparent $K_D$ for this interaction was slightly weaker than ESAT-6
156 self-association at neutral pH, but the total amount of binding was 20-30-fold greater, suggesting
157 that low pH conditions trigger ESAT-6 to assemble into larger complexes. Further, there have
158 been conflicting reports on whether ESAT-6 and CFP-10 dissociate from each other at low pH (de
159 Jonge et al., 2007; De Leon et al., 2012; Lightbody et al., 2008). Our results support the stable
160 interaction of ESAT-6 and CFP-10 at low-pH (Fig 3F), which exhibits an extremely tight apparent
161 $K_D$ of 0.4 pM at pH 4.5: however, this is likely due to the multivalent ESAT-6 self-association
162 occurring in this condition (Fig 3G). To determine the precise pH at which ESAT-6 self-association
163 becomes dominant, we performed BLI experiments at half pH units from 4.5 to 6.5 (Fig 3H). We
164 found that 5.0 was the most basic pH at which increased self-association occurred.

## 165 Formation of large ESAT-6 complexes at pH 4.5

166 The response from pH 4.5 ESAT-6 biosensors appeared to increase past the typical
167 association time of our BLI assay. Because of this, we extended the binding time to 20 minutes

168 (Fig 4A), but the increasing self-association of ESAT-6 continued at roughly the same rate
169 throughout. To explore the possibility of complex formation and to determine the timeframe over
170 which this occurs, we next performed turbidity assays in which 50 μM of either ESAT-6 or CFP-
171 10 were brought to pH 4.5 or 7.5 and $A_{350}$ was measured by plate reader for 1 hour (Fig 4B). We
172 observed an increase in turbidity at pH 4.5 but not 7.5 which was greater for ESAT-6 than CFP-
173 10, in line with previous findings (De Leon et al., 2012).

174 The BLI experiments we have shown thus far using the streptavidin-coated biosensors
175 (Fig 3A), have utilized ESAT-6 which had been biotinylated using succinimide chemistry
176 (ChromaLINK, Vector labs) allowing for precise quantification of incorporated biotin. Using 3 molar
177 equivalents of labeling reagent, we obtained ESAT-6 with an average of 0.99 biotins/protein.
178 However, succinimide chemistry can label any primary amine including the N-terminus and lysine
179 residues. ESAT-6 normally contains 3 lysines, and the pMRLB.7 construct contains 1 additional
180 lysine for a total of 4 (Fig 4C). Because it is unknown which region of the protein may be involved
181 in self-association, we generated an additional ESAT-6 construct capable of C-terminal site-
182 directed biotinylation via sortase-mediated transpeptidation via an LPETG motif (Fig 4C)
183 (Guimaraes et al., 2013; Popp et al., 2009). We performed additional BLI experiments using the
184 ESAT-6-LPETG construct and were able to verify similar behavior at neutral and acidic pH (Fig
185 4D-F).

## 186 Stoichiometry of ESAT-6 complexes

187 We next visualized the large ESAT-6 complexes by fluorescence microscopy in order to
188 get an idea of their scale. We mixed unmodified ESAT-6 with ESAT-6-LPETG-Biotin at a 10:1 ratio
189 and incubated on a poly-lysine coated coverslip, fixed, then stained with streptavidin-AF488 to
190 visualize ESAT-6 complexes. Fluorescence microscopy shows the development of individual
191 strands with the appearance of a heavily kinked thread or beads on a string (Fig 5A). These
192 structures were not present at neutral pH or when 6M guanidine was added to acidified ESAT-6.

193 To analyze the stoichiometry of these complexes, we next performed SEC coupled with
194 multi-angle light scattering (MALS), which can measure the molecular weight of complexes as
195 they elute from the SEC column. At pH 7.5, we observed a single peak with an approximate
196 molecular weight of 21 kDa, which most likely corresponds to an ESAT-6 homodimer (Fig 5B).
197 We did not observe the presence of any monomeric ESAT-6, indicating that it likely self-pairs in
198 the absence of CFP-10. This agrees with our BLI results from (Fig 3C). At pH 4.5, we were
199 surprised to see a single, well-defined peak at 46 kDa, most likely corresponding to a tetramer
200 (Fig 5C). No measurable monomer, dimer, or higher molecular weight complexes were observed.
201 While it is not surprising that the high molecular weight complexes observed (Fig 5A) were unable
202 to traverse the SEC column intact, it was unexpected that tetramers would be the only species
203 observed.

204 To address the question of the likely conformation of the homodimer and tetramer, we
205 performed modeling experiments using docking followed by molecular dynamics (MD) simulations
206 to estimate the most stable conformations. We started with a homology model based on
207 previously reported structures of the ESAT-6/CFP-10 heterodimer (PDB: 3FAV, 4J11, 4J7K, 4J10
208 and 4J7J) (Fan et al., 2015; Poulsen et al., 2014). To estimate the structure of the ESAT-6
209 monomer, we then performed a molecular dynamics simulation to observe the structural stability
210 of the protein's conformation. We observed that the energy-minimized structure of monomeric
211 ESAT-6 strongly resembles its conformation in the heterodimer. The helix-turn-helix structure
212 exhibits strong amphipathic nature, with both helices aligning to form a hydrophobic face flanked
213 by charged residues (Fig 5D).

214 We next modeled an ESAT-6 homodimer, starting again with a homology model based on
215 the heterodimer followed by a molecular dynamics simulation. The homodimer model showed
216 head-to-tail alignment of the ESAT-6 monomers associating via their hydrophobic faces and

217 stabilized on either side by salt bridges (Fig 5E). This homodimer model represents a likely
218 conformation of the species observed in the pH 7.5 SEC-MALS experiment (Fig 5B).

219 To model the tetrameric species observed in the acidic SEC-MALS experiment (Fig 5C),
220 we performed docking of ESAT-6 homodimers and then a molecular dynamics simulation of the
221 lowest energy conformation observed in docking. We observed the dimers interacting in a head-
222 to-tail orientation via their hydrophilic faces, supported by salt bridges (Fig 5F). In the tetramer
223 model, some of the charged residues, such as $Lys_{67}$, which had previously supported the dimer
224 interface, switched orientations to support the tetramer interface.

225 For each of these models, the molecular dynamics informs us about the proteins'
226 conformational stability. The root mean square fluctuation (RMSF) quantifies the amount of
227 movement along the peptide backbone for each residue, with lower values equating to more
228 stability. We performed molecular dynamics experiments for ESAT-6 in monomer, dimer, and
229 tetramer forms in order to evaluate the stability of each species (Fig 5G). In general, the α-helices
230 of ESAT-6 are stable, while the C- and N-termini are highly flexible. However, in the monomeric
231 form, the residues between 20 and 50 exhibit increased flexibility at pH 7.5. At pH 4.5, the
232 monomeric form exhibits increased flexibility along a majority of the backbone. At both pH values,
233 dimerization (and tetramerization) result in greater overall stability. At pH 7.5, the average RMSF
234 of the monomer is 2.51, which reduces to 2.33 for the dimer due to the reduced flexibility between
235 residues 20 and 50. The tetramer is only marginally more stable, at 2.27. At pH 4.5, the difference
236 between each state is even more pronounced, with an RMSF of 2.74, 2.04, and 1.94 for the
237 monomer, dimer, and tetramer, respectively.

## 238 Generation and characterization of an ESAT-6 specific nanobody

239 We generated an ESAT-6-specific alpaca-derived nanobody using our previously reported
240 phage display method (Alfadhli et al., 2021; Bachran et al., 2017; Weinstein et al., 2022). E11rv

241 was generated by immunization and panning against pMRLB.7 ESAT-6. Following initial isolation,
242 we performed biochemical characterization, starting with ELISA experiments to determine the
243 $EC_{50}$ of E11rv, which was found to be 1.26 μM (Fig 6A). We then determined the binding kinetics
244 via BLI, which we performed on both pMRLB.7 ESAT6 as well as our ESAT-6-LPETG construct
245 to ensure that the tag was not essential for binding (Fig 6B-C). E11rv bound similarly to ESAT-6
246 and ESAT-6-LPETG with $K_D$s of 331 nM and 376 nM, respectively.

247 To determine the binding site, we performed hydrogen deuterium exchange experiments
248 with ESAT-6 (Harris et al., 2023; Masson et al., 2019; Rathinaswamy et al., 2021). This involves
249 incubating either apo or E11rv-bound ESAT-6 in $D_20$ buffer for different lengths of time. The
250 deuterium will exchange with acidic protons in the protein at different rates depending on the
251 solvent exposure, giving insights into which areas of the protein are more tightly folded, or
252 shielded by protein-protein interactions with a nanobody (Fig 6D). Digestion followed by MS
253 allows quantification of the extent of deuteration along the peptide backbone and concomitant
254 binding site estimation. For E11rv, we observed decreased deuteration compared to apo around
255 positions 50-65 (on the C-terminal helix, near the loop), and to a lesser extent positions 98-110
256 (within the tag). The region between these segments, from residues 66-94, displayed an increase
257 in solvent exposure, as did residues 14-28, on the opposing helix directly across from 66-94. A
258 likely explanation for this pattern is that E11rv binds around residues 50-65, and that this somehow
259 destabilizes the C-terminal portion of the helix or separates the helices enough to allow more
260 solvent exposure between helices. It is unclear how the small region within the tag might be
261 involved, but Fig 6B suggests that the positioning of the tag has little impact on binding, and this
262 region is predicted to be largely unstructured.

## 263 E11rv inhibits Mtb replication in macrophages.

264 We next performed functional testing of E11rv using two complementary approaches for
265 measuring the growth and viability of internalized Mtb in macrophages. The first of these

266 experiments used a live/dead reporter strain of Mtb based on H37Rv which constitutively
267 expresses mCherry and dox inducible expression of GFP, which has been shown to correlate with
268 CFU count (Martin et al., 2012). We infected THP-1 cells with live/dead reporter Mtb pre-incubated
269 with E11rv or an isotype control, then allowed the infection to proceed for 3 days before inducing
270 GFP with doxycycline for 24 hours. After fixing and staining for actin to reveal the location of cells,
271 we performed fluorescence microscopy on the infected cells. We then used CellProfiler to identify
272 all Mtb within images by their red fluorescence and calculated the GFP/RFP ratio for each
273 identified bacterium (Stirling et al., 2021). In this experiment, we found that E11rv led to a
274 statistically significant reduction in Mtb viability (Fig 6F,G).

275 The second functional assay we performed was based on continuous growth
276 measurement of luminescent LuxABCDE-expressing Mtb (Andreu et al., 2010; Leddy et al.,
277 2023). We prepared stable THP-1 cell lines with cytoplasmic expression of E11rv or an isotype
278 nanobody. We then infected the nanobody-expressing THP-1 cells with luminescent Mtb and
279 monitored their growth continuously via plate reader for 5 days, and we found that E11rv reduced
280 the growth rate substantially (Fig 6H). Over the full 5 days, the isotype-expressing cells allowed
281 the Mtb to grow to 6-fold over its starting value while the E11rv-expressing cells reduced this to
282 just under 3-fold.

## 283 Discussion

284 This study has several key findings. Firstly, ESAT-6 undergoes rapid self-association into
285 large complexes at pH levels below 5.0, and this may be preceded by formation of stable
286 tetramers. Second, in the absence of CFP-10, ESAT-6 exists as a homodimer at neutral pH. Third,
287 our nanobody, E11rv, binds to ESAT-6 and can inhibit the growth of Mtb inside cells when treated
288 externally or via cytoplasmic expression.

289 The issue of incomplete information about the amino acid sequence of one of the most
290 widely used ESAT-6 constructs is surprising, but none of the data we have generated suggested
291 a practical difference with differently tagged constructs. Previous studies have found major
292 differences in function between recombinant ESAT-6 in general when compared with “native”
293 ESAT-6 purified from Mtb cultures, which are typically purified using much harsher techniques
294 than recombinant protein due to the lack of affinity tags. One attractive theory for the observed
295 difference between recombinant and native ESAT-6 which is gaining traction is N-terminal
296 acetylation being required for ESAT-6 function, but this has not yet been proven in Mtb infection
297 (Aguilera et al., 2020; Collars et al., 2023; Mba Medie et al., 2014; Okkels et al., 2004). The most
298 commonly given reason for the importance of N-acetylation is that acetylated ESAT-6 is more
299 easily released from CFP-10 under acidic conditions. Our results suggest that purified ESAT-6
300 exists in a dimerized state in the absence of CFP-10, but our Native-PAGE (Fig 2A) and SEC (Fig
301 1C) demonstrate that purified ESAT-6 has no trouble interacting with CFP-10 to form a 1:1
302 complex. It is unclear whether the observed 1:1 complex is an ESAT-6/CFP-10 heterodimer
303 formed by exchange between ESAT-6 and CFP-10 homodimers, or if we are instead observing
304 formation of a tetramer composed of one each ESAT-6 and CFP-10 homodimers. Further, our low
305 pH BLI results (Fig 3F) suggest that self-associated ESAT-6 has no difficulty interacting with CFP-
306 10.

307 Our modeling and SEC-MALS data suggest that ESAT-6 can interact with itself using both
308 of its faces, one of which is hydrophobic, and one of which is hydrophilic; and both of which are
309 supported by salt bridges formed by charged residues at either edge. This implies that ESAT-6
310 may still be able to self-associate within membranes via its hydrophilic face. This agrees with the
311 putative requirement for compartment acidification in order to drive membrane damage, as our
312 data suggests that low pH is required for self-association at this interface, but likely does not affect
313 the hydrophobic interface, which must then require a different mechanism for dissociation and

314 membrane insertion. Some have suggested that other mycobacterial factors may help facilitate
315 the membrane insertion of ESAT-6, such as phthiocerol dimycocerosates (Augenstreich et al.,
316 2020, 2017).

317 Modeling approaches have also been used previously to propose an organized ESAT-6
318 pore structure using similar logic, but these have yet to be supported by physical evidence (Karki
319 et al., 2020; Refai et al., 2015). However, there is precedent for ESAT-6-like WXG proteins to form
320 organized membrane channels, with a recent study demonstrating a pentameric EsxE/EsxF
321 structure capable of membrane insertion and toxin trafficking (Tak et al., 2021). Critically, EsxE
322 does not dissociate from EsxF in order to insert into the membrane. Such structures have yet to
323 be observed with ESAT-6/CFP-10, but this may just be a matter of finding the appropriate
324 conditions and reagents.

325 Finding molecular tools to interrogate the function of Mtb virulence factors remains a
326 challenge due to the complexity of accessing Mtb in its native environment within the phagosome.
327 The nanobody described here presents a novel way of targeting the bacteria *in situ*, which we
328 demonstrated by modulating its growth using intracellularly expressed E11rv. Because E11rv
329 showed functional effects both when added in the media and when expressed inside the cell
330 cytoplasm, it suggests a significant amount of communication between Mtb inside the phagosome
331 and other compartments of the cell. This is consistent with the findings of many other studies
332 which show numerous putative activities for ESAT-6 such as induction of apoptosis (Behura et
333 al., 2019; Choi et al., 2010; Lim et al., 2016; Yang et al., 2015), inhibition of interferon-γ production
334 (Kumar et al., 2012; Peng et al., 2011), inhibition of autophagy (Dong et al., 2016; Romagnoli et
335 al., 2012; Yabaji et al., 2020), inhibition of antigen presentation (Sreejit et al., 2014), induction of
336 type I interferon (Jang et al., 2018; Lienard et al., 2020), and a more recent study showing an
337 ESX-1-dependent mechanism for incorporation of Mtb antigens into MHC-I presentation via
338 cytosolic antigen processing (Leddy et al., 2023). Whereas most of these functions rely only on

339 secretion of ESAT-6 into the cytoplasm, the ability of E11rv to access Mtb suggests that this
340 communication is likely two-way.

## 341 Author Contributions

342 Timothy A Bates: Conceptualization, Methodology, Validation, Formal Analysis, Investigation,
343 Data Curation, Writing – Original Draft, Writing – Review & Editing, Visualization, Supervision,
344 Project Administration, Funding acquisition.

345 Mila Trank-Greene: Conceptualization, Methodology, Validation, Investigation, Data Curation,
346 Writing – Review & Editing, Visualization.

347 Xammy Nguyenla: Methodology, Investigation, Writing – Review & Editing.

348 Aidan Anastas: Methodology, Investigation.

349 Ilaria R Merutka: Methodology, Investigation.

350 Shandee D Dixon: Methodology, Investigation.

351 Anthony Shumate: Methodology, Investigation, Writing – Review & Editing.

352 Abigail R Groncki: Methodology, Investigation.

353 Matthew AH Parson: Methodology, Software, Validation, Formal Analysis, Investigation, Data
354 Curation, Visualization.

355 Eric Barklis: Conceptualization, Methodology, Writing – Review & Editing.

356 John E Burke: Conceptualization, Formal Analysis, Resources, Supervision, Project
357 Administration.

358 Ujwal Shinde: Conceptualization, Methodology, Software, Validation, Formal Analysis,
359 Investigation, Data Curation, Writing – Review & Editing, Visualization.

360 Hidde L Ploegh: Conceptualization, Resources, Writing – Review & Editing.

361 Fikadu G Tafesse: Conceptualization, Methodology, Validation, Formal Analysis, Resources,
362 Writing – Original Draft, Writing – Review & Editing, Supervision, Project Administration, Funding
363 acquisition.

## 364 Acknowledgements

365 This study was supported by the Bill & Melinda Gates foundation grant OPP1179922 (to FGT),
366 NIH R01AI141549 (to FGT), Silver Family Innovation Fund (to FGT), NHLBI training grant
367 5T32HL083808 (to TAB). BLI data were generated on an Octet Red 384, which is made available
368 and supported by the OHSU Biophysics Shared Resources Core and equipment grant number
369 S10OD023413. Mass spectrometry experiments were performed with support from Dr. Larry L.
370 David and the OHSU Proteomics Shared Resource core.

## 371 Competing interests

372 HLP serves as an advisor to and owns stock in Cerberus Therapeutics. HLP serves as a
373 consultant to Johnson and Johnson, Immatics Therapeutics, Cue Biopharma, Revela
374 Therapeutics, and Tiba Bio. JEB reports personal fees from Scorpion Therapeutics, Reactive
375 therapeutics and Olema Oncology; and research grants from Novartis. All other authors declare
376 that they have no competing interests.

# 377 Methods

## 378 Plasmids and primers

### 379 Plasmids

| Name | Description | Source |
|---|---|---|
| pMRLB.7 | ESAT-6 expression vector | BEI Resources, NR-50170 |

| | | |
|---|---|---|
| pMRLB.46 | CFP-10 expression vector | BEI Resources, NR-13297 |
| pMRLB.7-LPETG | ESAT-6-LPETG expression vector | This study |
| pHEN | Nanobody expression vector | (Hoogenboom et al., 1991) |
| pInducer20 | Lentiviral expression vector | (Meerbrey et al., 2011) |

380 ## Primers

| Name | Sequence |
|---|---|
| T7 (sequencing primer) | TAATACGACTCACTATAGGG |
| ESAT-6-Fw | CCGGAAACCGGCGGCATCAAGCTTATCGATACCGTCGACCTC |
| ESAT-6-Rv | GCCGCCGGTTTCCGGGAGCTCTGCGAACATCCCAGTG |

381 ## Cloning ESAT-6-LPETG

382 ESAT-6-LPETG was generated by in vivo assembly (IVA) as described previously (García-
383 Nafría et al., 2016). PCR was performed on pMRLB.7 using ESAT-6-Fw and ESAT-6-Rv primers
384 using Q5 polymerase with the following recipe and cycle design. Reactions were treated with DpnI
385 for 15 minutes at 37°C. 2 µL of reaction mixture was added directly to 50 µL of chemically
386 competent DH5-α cells, incubated on ice for 30 minutes, heat shocked at 42 for 30 seconds, then
387 immediately added to 200 µL of SOC, after which it was recovered for 30 minutes at 37°C and
388 plated on Luria Bertani (LB)-ampicillin (amp) agar plates, and incubated overnight at 37°C. Clones
389 were sequence confirmed before further use.

390 ## Expression and purification of ESAT-6 and CFP-10

391 pMRLB.7, pMRLB.46, and pMRLB.7-LPETG were transformed into *Escherichia coli* BL21
392 Rosetta rare codon competent cells. 25 mL Luria Bertani (LB) starter cultures were grown
393 overnight at 37°C with shaking with 100 ug/mL ampicillin to stationary phase. Each starter culture
394 was used to inoculate 1L of LB, which was then grown at 37°C until reaching an $OD_{600}$ of 0.8, at
395 which point it was induced with 0.1 mM IPTG for 4 hours at 37°C. Bacteria was pelleted by

396 centrifugation at 6,000×g for 10 minutes, then frozen at –80°C. Pellets were thawed and
397 resuspended in 25 mL of 10 mM Tris HCl, 300 mM NaCl, 10% glycerol, 10 mM Imidazole, 1 ug/mL
398 DNase and RNase, 0.5 mg/ml Lysozyme, 10 mM DTT, and 1 tablet/100 mL Sigma fast EDTA free
399 protease inhibitor (Lysis buffer) for 20 minutes. Lysates were sonicated on ice for 30 seconds on
400 and 30 seconds off for a total of 5 minutes. Crude lysates were then clarified by centrifugated at
401 20,000×g for 20 minutes. Supernatant was decanted and spun again similarly. Ni-NTA beads were
402 washed with 10 mM Tris HCl, 300 mM NaCl, 10 % glycerol (wash buffer). Lysate was applied to
403 0.5 mL of Ni-NTA beads per liter of bacteria and rocked for 1 hour at 4°C then poured over a 25
404 mL chromatography column. The column was then washed with 10 column volumes of wash
405 buffer plus 10 mM Imidazole, and then eluted in 10 mL wash buffer plus 250 mM Imidazole.
406 Protein containing fractions (assessed by SDS-PAGE) were pooled and imidazole was then buffer
407 exchanged and concentrated with 3 kDa MWCO centrifugal concentrator. Protein concentration
408 was assessed by $A_{280}$, correction for extinction coefficient. Purity was determined by SDS-PAGE,
409 and α-$His_6$ western blot.

## 410 Western blot

411 15% SDS-PAGE gels were run with 1 µg of protein, and transferred to a PVDF membrane
412 (0.2 µm pore size) for 1 hour at 4°C, using a wet transfer tank (Trans-blot, Bio Rad). The
413 membrane was rinsed with deionized (DI) water and blocked with 2% non-fat dry milk (Lab
414 Scientific #978-907-4243) in tris buffered saline with 0.1% Tween-20 (TBST) for 30 minutes at
415 room temperature (RT). Blots were stained with 1:10,000 α-$His_6$-HRP (Invitrogen, MA1-80218) in
416 blocking buffer overnight at 4°C. Blots were then washed with PBST three times for 5 minutes
417 each. Signal was developed using SuperSignal Western Pico PLUS (Thermo Scientific)
418 chemiluminescent substrate according to the manufacturer's instructions and visualized on an
419 ImageQuant LAS 4000.

420 ## Size exclusion chromatography (SEC)

421 SEC was performed on a HiLoad 16/600 Superdex 75 pg (Cytiva) column on an
422 ÄKTApurifier FPLC (GE) system. Sterile filtered and degassed 10 mM Tris HCl, 300 mM NaCl, 10
423 % glycerol, pH 7.8 was used as a mobile phase and was run at 0.8 mL/min at 4°C. Data was
424 collected with Unicorn 5.31 (GE).

425 ## Native polyacrylamide gel electrophoresis (PAGE)

426 15% polyacrylamide gels were cast with 3.5 mL 30% acrylamide:0.8% bis-acrylamide,
427 1.7mL of 1.5 M Tris HCl buffer, 70 µL of 10% ammonium persulfate, and 7 µL of TEMED per gel.
428 To analyze the dimerization of CFP10 and ESAT6, 25 µM stocks of each protein were made,
429 mixed in varying ratios, and incubated for 60 minutes at 4 C. Non-denaturing loading buffer was
430 added and reactions were loaded then run at 4°C overnight at 50 V in Tris-Glycine buffer without
431 SDS (National Diagnostics) and then Coomassie stained.

432 ## Hemolysis

433 ### Bacterial hemolysis

434 Hemolysis experiments were performed as described previously (Conrad et al., 2017).
435 Sheep blood (HemoStat labs, SBC100) was washed with PBS by centrifugation at 3200×g for 5
436 minutes and resuspended to a final concentration of 1% (v/v) red blood cells (RBC) in PBS.
437 Bacterial cultures, Mm, Mtb, MtbΔRD1 were grown in Middlebrook 7H9 with OADC to an $OD_{600}$
438 between 0.3 and 1.0. Cultures were washed with PBS by centrifugation at 500×g for 5 minutes
439 and resuspended in PBS. The equivalent of 3 mL of culture at $OD_{600}$ 1.0 was resuspended in 100
440 µL of PBS and combined with 100 µL of 1% RBCs. Centrifuged samples at 3200×g for 5 minutes,
441 then incubated the pelleted samples at 37°C for Mtb and MtbΔRD1, or 33°C for Mm for 2 hours.
442 Samples were then resuspended by pipette and spun again similarly. The absorbance at 405 nm
443 was measured for each sample using a plate reader, as well as for samples without bacteria and

444 samples with 0.1% Triton-X100. Percent hemolysis was calculated as ($A_{405}$Sample – $A_{405}$PBS) ÷
445 ($A_{405}$Triton – $A_{405}$PBS) × 100.

## 446 Protein hemolysis

447 For measurement of protein hemolysis, RBCs were resuspended to 1% (v/v) in McIlvaine
448 buffer of pH 4.5, 5.5, 6.5, 7.5, and 8.5 prepared as previously described (McIlvaine, 1921). 100
449 µL of 1 mg/mL ESAT-6 was combined with 100 µL of 1% RBC solution and incubated at RT for 1
450 hour. Samples were then spun at 3200×g for 5 minutes and the $A_{405}$ supernatants were measured
451 by plate reader. PBS and Triton samples were prepared similarly to bacterial hemolysis, and %
452 hemolysis was calculated using the same formula.

## 453 Biolayer interferometry (BLI)

454 BLI was performed using an Octet Red384 machine (ForteBio). Octet Streptavidin
455 Biosensors (Sartorius, #18-5019) were used for all experiments. Biotinylated proteins were
456 prepared using the succinimide (ESAT-6, CFP-10, RBD) or sortase (ESAT-6-LPETG, E11rv, VHH
457 52) method. Recombinant SARS-Cov-2 spike RBD was used as a loading control for ESAT-6 and
458 CFP-10 experiments, while VHH 52 against influenza was used as a loading control for E11rv
459 experiments. For all experiments, Biosensors were soaked for 20 minutes in DI water, blocked for
460 30 seconds in 10mM Citrate, 100mM NaCl, 3mM EDTA, 0.1% BSA, 0.005% Tween-20 (running
461 buffer) which was adjusted to match the pH of the test condition (4.5, 5.0, 5.5, 6.0, or 7.5).
462 Biotinylated protein was then loaded onto the biosensors until approximately 1 nm of binding
463 response was observed. Excess protein was washed off with three cycles of 15 seconds in 10
464 mM glycine pH 1.7 then 15 seconds in running buffer. Washing was followed by a 30 second
465 baseline step in running buffer, an association step with test analyte diluted in running buffer, then
466 dissociation step in plain running buffer. When multiple conditions were tested, the lowest
467 concentration was tested first, and 3 wash cycles were performed between conditions. Loading
468 control biosensors followed the same protocol with identical sample concentrations. Data was

469 collected with Octet Data Acquisition 10.0.0.87 (ForteBio), and data was analyzed with Octet Data
470 Analysis HT 10.0.0.48 (ForteBio). Background subtraction was performed using loading control
471 biosensors, data was aligned to the average of the baseline step, and smoothed by Savitzky-
472 Golay filtering. All data were fit to a 1:1 model using the "full (assoc and dissoc) setting" using the
473 entire step length. Reported kinetic binding constants ($K_D$, $K_{ON}$, and $K_{OFF}$) values were calculated
474 by taking the geometric mean of binding constants calculated for individual conditions and
475 replicates. Conditions were excluded from the average when the Data Analysis HT software was
476 unable to calculate all constants for a given condition due to insufficient signal. The only conditions
477 excluded using this criterion were ESAT-6 pH 7.5 self-association at 0.316 nM, and E11rv
478 association with ESAT-6 and ESAT-6-LPETG at 0.33 and 0.1 μM.

## 479 Turbidity assay

480 ESAT-6 was buffer exchanged into PBS using a Zeba spin column (ThermoFisher) and
481 diluted to a concentration of 50 μM. 30 μL of ESAT-6 was added to each well in a 384 well plate.
482 To each well, 2 μL of either PBS or Citrate buffer was added. Citrate buffer contained 50mM citric
483 acid and 100 mM NaCl, and was adjusted for pH such that mixing 5mL buffer with 45mL PBS
484 resulted in a solution with pH 4.5. Plates were immediately added to a plate reader following pH
485 adjustment and $A_{350}$ was read every 2 minutes for a total of 60 minutes with 10 seconds of shaking
486 between each read. Turbidity was calculated as $A_{350}$Sample – $A_{350}$PBS.

## 487 Biotinylation

### 488 Succinimide biotinylation

489 Recombinant ESAT-6, CFP-10, and RBD (lacking an LPETG tag) were biotinylated using
490 the ChromaLINK biotinylation kit (Vector labs). Manufacturer's instructions were used. 3 molar
491 equivalents of biotinylation reagent yielded a labeling level of 0.99 biotins/protein calculated using
492 the E1% method in the manufacturer's labeling calculator. Proteins were buffer exchanged into

493 PBS by passing through a PBS-equilibrated Zeba desalting column (ThermoFisher, 89882).
494 Protein aliquots were snap frozen in liquid nitrogen and stored at -80°C until use.

## 495 Sortase biotinylation

496 ESAT-6-LPETG and LPETG-tagged nanobodies were C-terminally biotinylated using
497 sortase as previously described (Guimaraes et al., 2013; Popp et al., 2009). Briefly, 20 µL of 20
498 mg/mL sortase enzyme, 20 µL of 10 mM GGG-Biotin peptide, and 200 µL of 1mg/mL LPETG-
499 labeled protein. This mixture was incubated at 4°C overnight, then added to 50 uL of packed,
500 PBS-washed Ni-NTA beads to remove the His-tagged sortase enzyme and any unreacted protein
501 for 2 hours at 4°C. The resulting supernatant was buffer exchanged into PBS by passing through
502 a PBS-equilibrated Zeba desalting column (ThermoFisher, 89882). Protein aliquots were snap
503 frozen in liquid nitrogen and stored at -80°C until use.

## 504 Protein microscopy

505 Coverslips were coated in poly-L-Lysine at 4°C overnight, washed once with PBS, then
506 dried before use. A 9:1 molar ratio of ESAT-6:ESAT-6-LPETG-Biotin (final concentration 0.24
507 mg/mL) was prepared prior to addition of 10× citrate buffer prepared similarly to the turbidity
508 assay. The guanidine-containing sample used a protein concentration of 0.7 mg/mL and included
509 a final concentration of 2M guanidine. The treated protein mixtures were incubated at RT for 30
510 minutes. Five 2µL drops were added to each coverslip and incubated at RT for 30 minutes.
511 Coverslips were fixed by addition of 4% formaldehyde in PBS for 30 minutes at RT, washed three
512 times with PBS, blocked in 2.5% BSA in PBS for 30 minutes at RT, washed 3 times with PBS,
513 stained with 1:10,000 (in PBS) streptavidin-AF488 (Jacskon Immuno, 016-540-084), and finally
514 washed 3 times with PBS. Coverslips were mounted onto microscope slides with Prolong Gold
515 antifade (ThermoFisher, P10144). Images were captured on a Zeiss LSM 980 with Airyscan2
516 using a 63× oil objective and processed with Zeiss Blue Airyscan joint deconvolution.

## Size exclusion chromatography multi-angle light scattering (SEC-MALS)

SEC-MALS was performed on an FPLC (GE) with a DAWN MALS detector (Wyatt) (Get description from Ujwal) was used. 100 µg of ESAT-6 was buffer exchanged with a Zeba spin column immediately prior to each experiment and injected onto a Superdex 75 increase 10/300 column at a flow rate of 0.5 mL/min at 4°C. The mobile phase was 10 mM Citrate, 300 mM NaCl, pH 4.5 or pH 7.5. Buffers were sterile filtered to 0.1 µm and degassed prior to use. Data analysis was performed using ASTRA software (Wyatt).

## Modeling

### Homology Modeling

The ESAT6 and CFP10 protein sequences were modeled via the Homology Modeling protocol in YASARA version 22.09.24. Sidechain optimization occurred through the FoldX plugin, with an energy minimization using AMBER14 force-field. X-ray structures with specified PDB IDs: 3FAV-A, 4J11-B, 4J7K-B, 4J10-A and 4J7J-B (PDB ID-Chain) served as templates for full-length modeling of both proteins, with alternative models considered if alignments were unclear. For CFP10, about 66% aligned with the template, and specific residues (MAEMKTDAAT and RADEEQQQAL) were predicted using loop modeling. Similarly, around 69% of ESAT6 aligned, with residues (STEGNVTGMF and MTEQQW) modeled as described earlier. After side-chain building and optimization, new model components underwent combined steepest descent and simulated annealing minimization. YASARA then integrated the best model parts to create a high-accuracy hybrid for each protein. Structures, dihedrals, and 1D to 3D packing were inspected for optimal monomer models. Dimer models were based on orientations from the 3FAV template, while tetrameric structures were predicted using dimer models as templates via the M-Zdock server.

540 ## Molecular Dynamic Simulations

541 The protonation status of amino acid residues and subsequent alteration of side-chain
542 interactions and the domain structure can be influenced by the pH, impacting the stability,
543 dynamics, and/or interactions of CFP10, ESAT6, and their heterodimers. As such, these were
544 examined at both pH 4.5 and 7.4 through molecular dynamics simulations. These simulations,
545 performed under the NPT ensemble with periodic boundary conditions, provided a sampling of
546 the conformational space available to the various oligomeric forms of ESAT6 and CFP10. The
547 domains were subjected to MD simulations for a period of 50 ns and snapshots were taken at 250
548 ps intervals for later examination. Each simulation process was run twice with distinct random
549 seeds to confirm the reliability of the simulations. The RMSF of each simulation was plotted as
550 displayed in the Figure.

551 ## Nanobody discovery

552 Nanobody discovery was performed as previously described (Weinstein et al., 2022).
553 Briefly, Alpacas were immunized with recombinant ESAT-6 protein and immune serum was
554 collected. Peripheral blood mononuclear cells (PBMC) were isolated and RNA was extracted with
555 an RNeasy mini kit (Qiagen 74104), which was then converted to cDNA using Superscript III
556 (Invitrogen 18080051). VHH genes were amplified using gene specific primers for long- and shot-
557 hinge heavy-chain-only antibodies (Maass et al., 2007). Amplified VHH genes were cloned into a
558 phagemid vector based on pCANTAB-5E and transformed into competent TG1 *E. coli*. The
559 bacterial library was infected with helper phage to generate a phage library and purified by PEG
560 precipitation (Frei and Lai, 2016). The phage library which was panned against recombinant
561 ESAT-6 to enrich strong binders. Panning consisted of incubating the purified phage library in
562 antigen-coated tubes and then eluting with pH 2.2 glycine. Eluted phage were neutralized with
563 1M Tris pH 9.1, and transferred to log-phase ER2738 *E. coli*, to produce the enriched library,
564 which was plated on agar. Individual ER2738 clones were selected and screened by ELISA to

565 quantify affinity. E11rv was selected for further testing based on its performance in the screening
566 ELISA, and was cloned into the pHEN periplasmic expression plasmid.

## 567 Nanobody purification

568 Nanobodies were purified by periplasmic purification. pHEN plasmid containing each
569 nanobody was transformed into *E. coli* WK6 competent cells. 20 mL starter cultures were grown
570 overnight at 37 C with shaking in Terrific Broth (2% tryptone, 1% yeast extract, 90mM phosphate)
571 with 100 ug/mL ampicillin to stationary phase. Starter cultures were used to begin 1L Terrific Broth
572 cultures to be grown at 37C. When cultures reached OD600 of approximately 0.6 OD, they were
573 induced with 1 mM IPTG overnight at 30 C. Bacteria was pelleted at 4,000 xg for 10 minutes and
574 resuspended in 40 mLs of lysis buffer (200 mM HEPES, 0.65 mM EDTA, 0.5 M sucrose, at cold
575 pH 8), then incubated at 4C for 1-2 hrs. Add 40 mLs of ice cold water and incubate for 2 hrs,
576 rotating, to lyse periplasm by osmotic shock. Periplasmic fraction was isolated by centrifuging
577 lysate at 8,000 xg for 15 minutes, twice. VHH E11 was purified with Ni-NTA chromatography.
578 Purified E11 was then buffer exchanged and concentrated with 3kDa cutoff centrifuge filters
579 (Millipore), then aliquoted and frozen for future use.

## 580 Enzyme linked immunosorbent assay (ELISA)

581 ELISA experiments were performed as described previously (Weinstein et al., 2022).
582 MaxiSorp plates (Invitrogen 442404) were coated with ESAT-6 at 5 µg/mL in PBS overnight at
583 4°C. Plates were blocked in 2% BSA, 2% Polyvinylpyrrolidone (PVP), 0.1% Tween-20 in PBS
584 (blocking buffer) for 30 minutes at RT. Dilutions of E11rv or isotype control VHH 52 were made in
585 blocking buffer and added to plates for 1 hour at RT with shaking. Plates were washed with PBST
586 3 times for 5 minutes each and biotinylated anti-VHH antibody (Jackson Immuno 128-065-232)
587 at 1:10,000 in blocking buffer was added for 1 hour at RT with shaking. Plates were washed again
588 and incubated with 1:10,000 streptavidin-HRP (Jackson Immuno 016-030-084) in blocking buffer
589 for 1 hour at RT. Plates were washed again and incubated with 50 µL of ODP (ThermoFisher

590 34006), prepared according to the manufacturer's instructions, for 15 minutes before stopping
591 with 50 µL of 2N $H_2SO_4$. $A_{492}$ was measured using a CLARIOstar PLUS (BMG) plate reader. Raw
592 data was background subtracted with wells lacking nanobody and normalized by dividing by the
593 highest binding well, then fit to a 4PL sigmoid curve in Prism 10.0.0 (Graphpad) to determine the
594 $EC_{50}$.

## 595 Hydrogen-deuterium exchange (HDX)

### 596 HDX-MS sample preparation

597 HDX reactions comparing ESAT6 Apo to E11rv-bound were carried out in 30 µl reaction
598 volumes containing 15 pmol of ESAT6. A protein mastermix was created for both reaction
599 conditions (500 nM ESAT6, 1 µM E11rv or equivalent volume of E11rv buffer). The exchange
600 reactions were initiated by the addition of 25 µL of $D_2O$ buffer (20 mM HEPES pH 7.5, 100 mM
601 NaCl) to 5 µL of protein mastermix (final $D_2O$ concentration of 78.6% [v/v]). Reactions proceeded
602 for 0.3s (3s on ice), 3s, 30s, 300s, and 3000s at 20°C before being quenched with ice cold acidic
603 quench buffer, resulting in a final concentration of 0.6M guanidine HCl and 0.9% formic acid post
604 quench. All conditions and timepoints were created and run in independent triplicate. Samples
605 were flash frozen immediately after quenching and stored at -80°C until injected onto the ultra-
606 performance liquid chromatography (UPLC) system for proteolytic cleavage, peptide separation,
607 and injection onto a QTOF for mass analysis, described below.

### 608 Protein digestion and MS/MS data collection

609 Protein samples were rapidly thawed and injected onto an integrated fluidics system
610 containing a HDx-3 PAL liquid handling robot and climate-controlled (2°C) chromatography
611 system (LEAP Technologies), a Dionex Ultimate 3000 UHPLC system, as well as an Impact HD
612 QTOF Mass spectrometer (Bruker). The full details of the automated LC system are described in
613 (Stariha et al., 2021). The samples were run over one immobilized pepsin column (Waters;
614 Enzymate Protein Pepsin Column, 300Å, 5µm, 2.1 mm X 30 mm) at 200 µL/min for 3 minutes at

615 2°C. The resulting peptides were collected and desalted on a C18 trap column (Acquity UPLC
616 BEH C18 1.7mm column (2.1 x 5 mm); Waters 186003975). The trap was subsequently eluted in
617 line with an ACQUITY 1.7 µm particle, 100 × 1 $mm^2$ C18 UPLC column (Waters), using a gradient
618 of 3-35% B (Buffer A 0.1% formic acid; Buffer B 100% acetonitrile) over 11 minutes immediately
619 followed by a gradient of 35-80% over 5 minutes. Mass spectrometry experiments acquired over
620 a mass range from 150 to 2200 m/z using an electrospray ionization source operated at a
621 temperature of 200°C and a spray voltage of 4.5 kV.

## 622 Peptide identification

623 Peptides were identified from a non-deuterated sample of ESAT6 using data-dependent
624 acquisition following tandem MS/MS experiments (0.5 s precursor scan from 150-2000 m/z;
625 twelve 0.25 s fragment scans from 150-2000 m/z). MS/MS datasets were analysed using PEAKS7
626 (PEAKS), and peptide identification was carried out by using a false discovery-based approach,
627 with a threshold set to 0.1% using a database of purified proteins and known contaminants. The
628 search parameters were set with a precursor tolerance of 20 ppm, fragment mass error 0.02 Da,
629 charge states from 1-8, leading to a selection criterion of peptides that had a -10logP score of
630 16.2.

## 631 Mass Analysis of Peptide Centroids and Measurement of Deuterium Incorporation

632 HD-Examiner Software (Sierra Analytics) was used to automatically calculate the level of
633 deuterium incorporation into each peptide. All peptides were manually inspected for correct
634 charge state, correct retention time, appropriate selection of isotopic distribution, etc. Deuteration
635 levels were calculated using the centroid of the experimental isotope clusters. Results are
636 presented as relative levels of deuterium incorporation and the only control for back exchange
637 was the level of deuterium present in the buffer (78.6%). Differences in exchange in a peptide
638 were considered significant if they met all three of the following criteria: ≥4.5% change in
639 exchange, ≥0.45 Da difference in exchange, and a p value <0.01 using a two tailed student t-test.

640 Samples were only compared within a single experiment and were never compared to
641 experiments completed at a different time with a different final $D_2O$ level. The data analysis
642 statistics for all HDX-MS experiments are in **Supplemental Table 1** according to the guidelines
643 of (Masson et al., 2019). The mass spectrometry proteomics data have been deposited to the
644 ProteomeXchange Consortium via the PRIDE partner repository (Perez-Riverol et al., 2022).

## 645 Imaging-based Mtb viability assay

646 Live/Dead H37rv Mtb constitutively express mCherry and have $Tet^{ON}$ inducible GFP
647 expression. THP-1 cells were seeded at 40,000 cells/well in glass bottom, black-walled 96 well
648 tissue culture plates and treated with 100 μM Phorbol-12-myristate-13-acetate (PMA) for 24 hours
649 prior to infection. Endotoxin free E11rv and unrelated isotype nanobodies were prepared to 1
650 mg/mL and sterile filtered prior to use. THP-1 cells were infected at an MOI of 1 with Live/Dead
651 Mtb was pre-incubated for 30 minutes with 100 μg/mL of nanobody. Infected plates were
652 incubated for 3 days in tissue culture conditions. Doxycyline was added to a final concentration
653 of 1 μg/mL and incubated for 24 hours. Plates were fixed with 5% formaldehyde in PBS for 1 hour
654 at RT in accordance with OHSU biosafety procedures before removing plates from the BSL3.
655 Plates were then washed with PBS and stained with Phalloidin-AF405 at 1:40 from 6.6 μM stock
656 for 1 hour. Wells were imaged with a Keyence (BZX-710) using a 20× S Plan Fluor ELWD lens.
657 49 images were captured for each well using the same exposure settings for each experiment.
658 Images were analyzed with CellProfiler 4.2.5 (Stirling et al., 2021). Images with obvious defects
659 such as large dust particles were excluded from the analysis. Mean GFP / Mean RFP was
660 calculated for each identified TB particle and the average GFP/RFP value was tabulated for each
661 image. Images were plotted as individual points in Prism (Graphpad) as described in the statistics
662 section.

663 ## Continuous luminescence viability assay

664 THP-1 cells were transduced with lentivirus to express nanobody-GFP fusion constructs
665 for E11rv and VHH 52 under a $Tet^{ON}$ promoter (pInducer20 plasmid). The lentiviruses were
666 generated as described previously (Niekamp et al., 2021). THP-1 cells were transduced and
667 selected with 600 µg/mL of G418 for 3 weeks, then maintained with 300 µg/mL G418 in every
668 other passage. For each experiment opaque white 96-well plates were seeded with 30,000
669 cells/well along with a matched clear plate, both including 100 nM PMA. Cells were incubated
670 with PMA for 24 hours before inducing with 1 µg/mL doxycycline for another 24 hours. Cell health
671 and nanobody expression was verified by microscopy of the clear plate. The opaque plate was
672 infected with bioluminescent pLux Mtb, which expresses the full luxABCDE cassette, at an MOI
673 of 1. The plate was sealed with a Beathe-Easy plate seal (Research Products International
674 248738) and put into a climate-controlled CLARIOstart plate reader for continuous luminescence
675 reading for 120 hours.

676 ## Statistics

677 Statistical analysis was performed in Prism 10.0.0 (Graphpad). In Figure 2B, two-tailed
678 one sample t-tests were performed with a significance cutoff of 0.05 against a hypothetical value
679 of 0. In figure 7B, a two-tailed unpaired t test was performed with a significance cutoff of 0.05. For
680 all plots, * = 0.05, ** = 0.01, *** = 0.001, **** = 0.0001.

681

682

683

# Figures

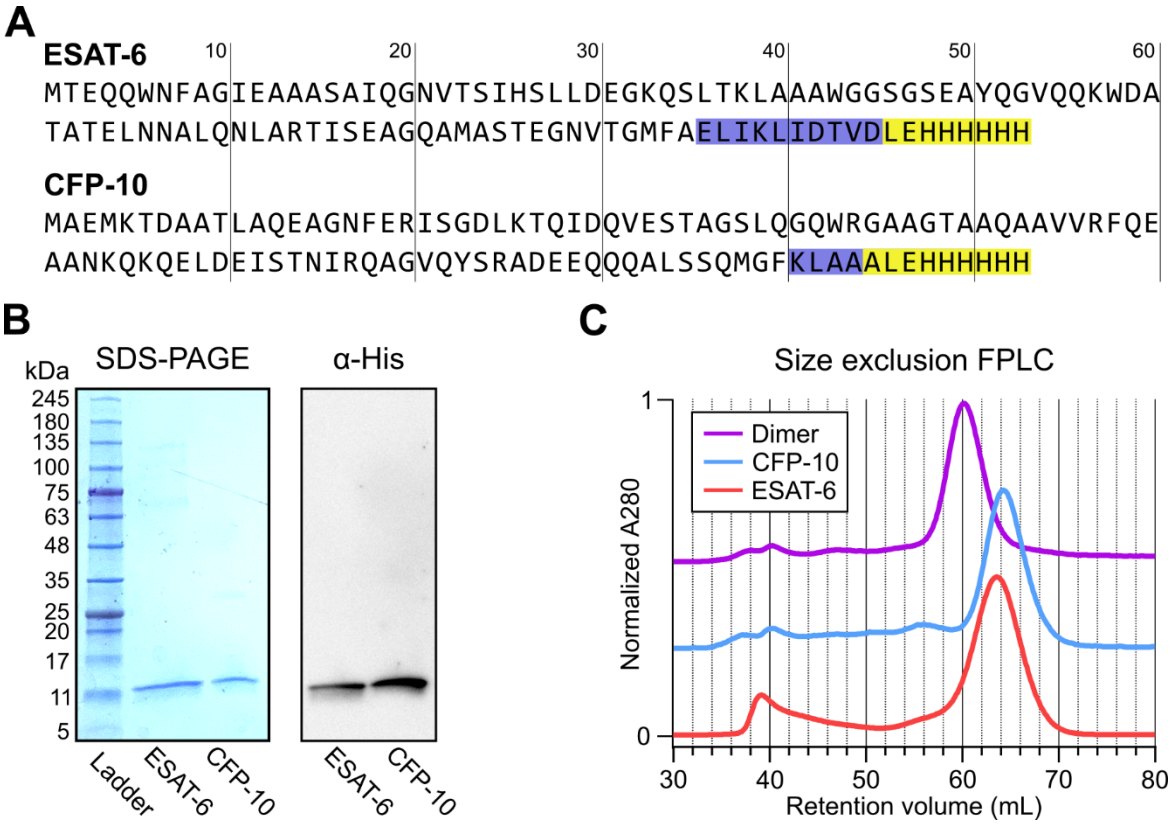


Figure 1: Expression of recombinant ESAT-6 and CFP-10. (A) amino acid sequences derived from plasmid sequencing of pMRLB.7 (ESAT-6) and pMRLB.46 (CFP-10) plasmids available from BEI Resources. The yellow highlights indicate the expected FALE-Histidine tag amino acid sequence while the blue highlights indicate unexpected additional amino acids. (B) SDS-PAGE gel of purified ESAT-6 and CFP-10 with a paired anti-$His_6$ western blot. (C) Size exclusion chromatography traces showing the retention volumes of purified ESAT-6, CFP-10 and an equimolar mixture of both (Dimer).

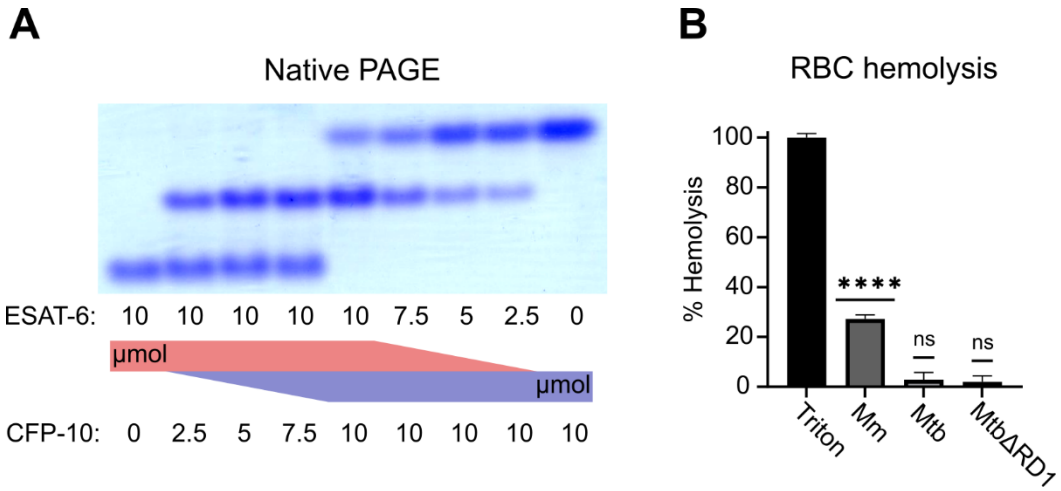


694

695 Figure 2: functional testing of ESAT-6 and CFP-10. (A) Native-PAGE analysis of ESAT-6 and
696 CFP-10 showing 1:1 complex formation at neutral pH. The displayed gel is representative of 3
697 replicates. (B) Contact-dependent red blood cell (RBC) hemolysis by whole bacteria, either
698 *Mycobacterium marinum* (Mm), *Mycobacterium tuberculosis* (Mtb), or Mtb with the region of
699 difference 1 deletion, incapable of producing ESAT-6 or CFP-10 (MtbΔRD1). Data in B represents
700 6 replicates. Statistical significance was determined using a one sample t test against a theoretical
701 mean of 0. * = 0.05, ** = 0.01, *** = 0.001, **** = 0.0001.

702

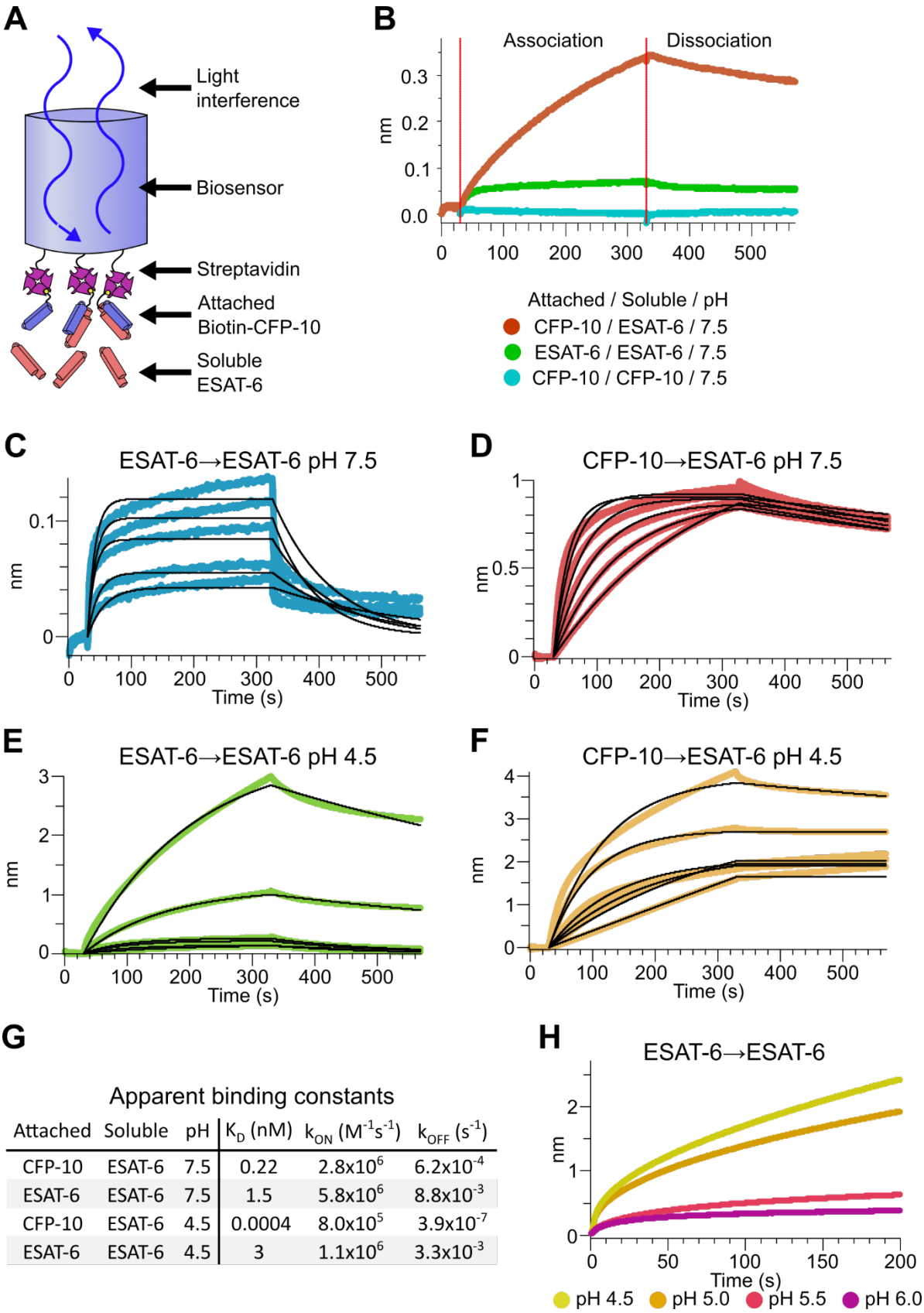


Apparent binding constants

| Attached | Soluble | pH | $K_D$ (nM) | $k_{ON}$ ($M^{-1}s^{-1}$) | $k_{OFF}$ ($s^{-1}$) |
|---|---|---|---|---|---|
| CFP-10 | ESAT-6 | 7.5 | 0.22 | $2.8 \times 10^{6}$ | $6.2 \times 10^{-4}$ |
| ESAT-6 | ESAT-6 | 7.5 | 1.5 | $5.8 \times 10^{6}$ | $8.8 \times 10^{-3}$ |
| CFP-10 | ESAT-6 | 4.5 | 0.0004 | $8.0 \times 10^{5}$ | $3.9 \times 10^{-7}$ |
| ESAT-6 | ESAT-6 | 4.5 | 3 | $1.1 \times 10^{6}$ | $3.3 \times 10^{-3}$ |

703

704 Figure 3: Binding kinetics of ESAT-6 and CFP-10 under neutral and acidic conditions. (A)
705 Biolayer interferometry (BLI) experimental design. Biotinylated ESAT-6 or CFP-10 are attached
706 to streptavidin coated biosensors, then dipped into solutions of free ESAT-6 or CFP-10. (B) BLI
707 experiment depicting ESAT-6 and CFP-10 association, ESAT-6 self-association, and CFP-10 self-
708 association at pH 7.5 with 50 μM. BLI experiment showing (C) ESAT-6 self-association at pH 7.5,
709 (D) CFP-10/ESAT-6 association at pH 7.5, (E) ESAT-6 self-association at pH 4.5, and (F) CFP-
710 10/ESAT-6 association at pH 4.5 Proteins in (C-F) were tested at 1, 3.16, 10, 31.6, and 100 μM.
711 (G) Table of apparent binding constants calculated with a 1:1 model for each indicated condition.
712 (H) BLI experiment testing ESAT-6 self-association at pH 4.5, 5.0, 5.5, and 6.0 with 100 μM
713 protein.

714

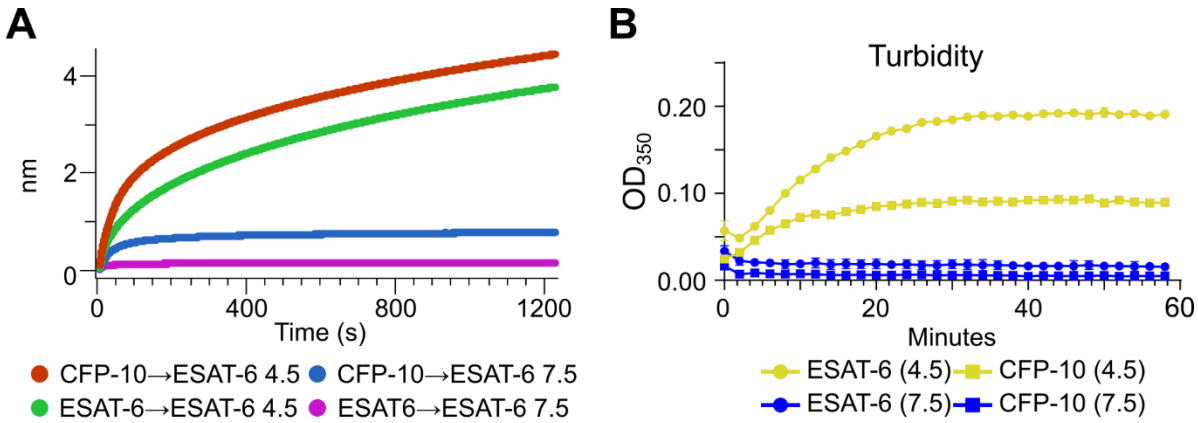


**C**

**ESAT-6-Lysine-Biotin (~1 biotin incorporated per protein)**

MTEQQWNFAGIEAAASAIQGNVTSIHSLLDEGKQSLTKLAAAWGGSGSEAYQGVQQKWDA
TATELNNALQNLARTISEAGQAMASTEGNVTGMFAELIKLIDTVDLEHHHHHH

**ESAT-6-LPETG (before sortase reaction)**

MTEQQWNFAGIEAAASAIQGNVTSIHSLLDEGKQSLTKLAAAWGGSGSEAYQGVQQKWDA
TATELNNALQNLARTISEAGQAMASTEGNVTGMFAELPETGGIKLIDTVDLEHHHHHH

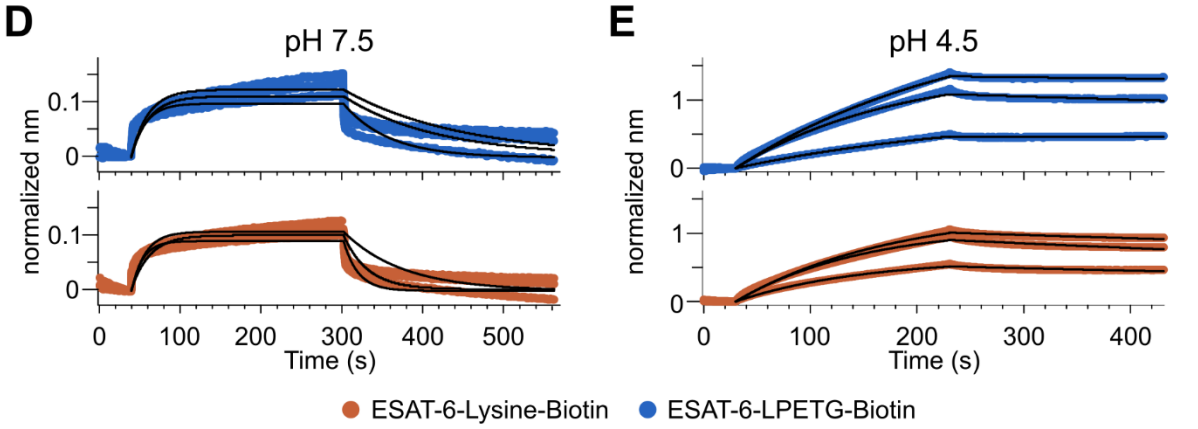


**F**

Apparent binding constants

| Attached | Soluble | pH | $K_D$ (nM) | $k_{ON}$ ($M^{-1}s^{-1}$) | $k_{OFF}$ ($s^{-1}$) |
|---|---|---|---|---|---|
| ESAT-6-LPETG-Biotin | ESAT-6 | 7.5 | 12 | $1.3x10^{6}$ | $1.6x10^{-2}$ |
| ESAT-6-Lysine-Biotin | ESAT-6 | 7.5 | 19 | $1.6x10^{6}$ | $3.1x10^{-2}$ |
| ESAT-6-LPETG-Biotin | ESAT-6 | 4.5 | 0.8 | $2.0x10^{5}$ | $1.7x10^{-4}$ |
| ESAT-6-Lysine-Biotin | ESAT-6 | 4.5 | 2.3 | $2.9x10^{5}$ | $6.8x10^{-4}$ |

Figure 4: Extensive self-association of ESAT-6. (A) BLI long-association experiment showing 50 μM ESAT-6 at pH 4.5 or 7.5 attaching to biosensors coated with either ESAT-6 or CFP-10. (B) Turbidity assay showing 50 μM ESAT-6 or 50 μM CFP-10 at pH 4.5 or 7.5 over time. Absorbance at 350nm read every 2 minutes. (C) Lysine-labeled Biotinylated ESAT-6 has an average of 1 biotin

720 per protein attached to the N-terminus or one of the orange highlighted lysine residues. The ESAT-
721 6-LPETG construct amino acid sequence is shown which includes and inserted LPETG motif, in
722 orange. Reaction with biotinylated poly-glycine via sortase-mediated transpeptidation results in
723 the teal highlighted residues being removed and replaced with a biotin molecule. BLI experiments
724 at (D) pH 7.5 and (E) pH 4.5 showing unmodified soluble ESAT-6 interacting with streptavidin
725 biosensor tips loaded with ESAT-6-Lysine-Biotin (red) or ESAT-6-LPETG-Biotin (blue). Curves
726 were normalized by dividing response values by the amount of protein added during the loading
727 step. (F) Summary of apparent kinetic binding constants in (D-E).

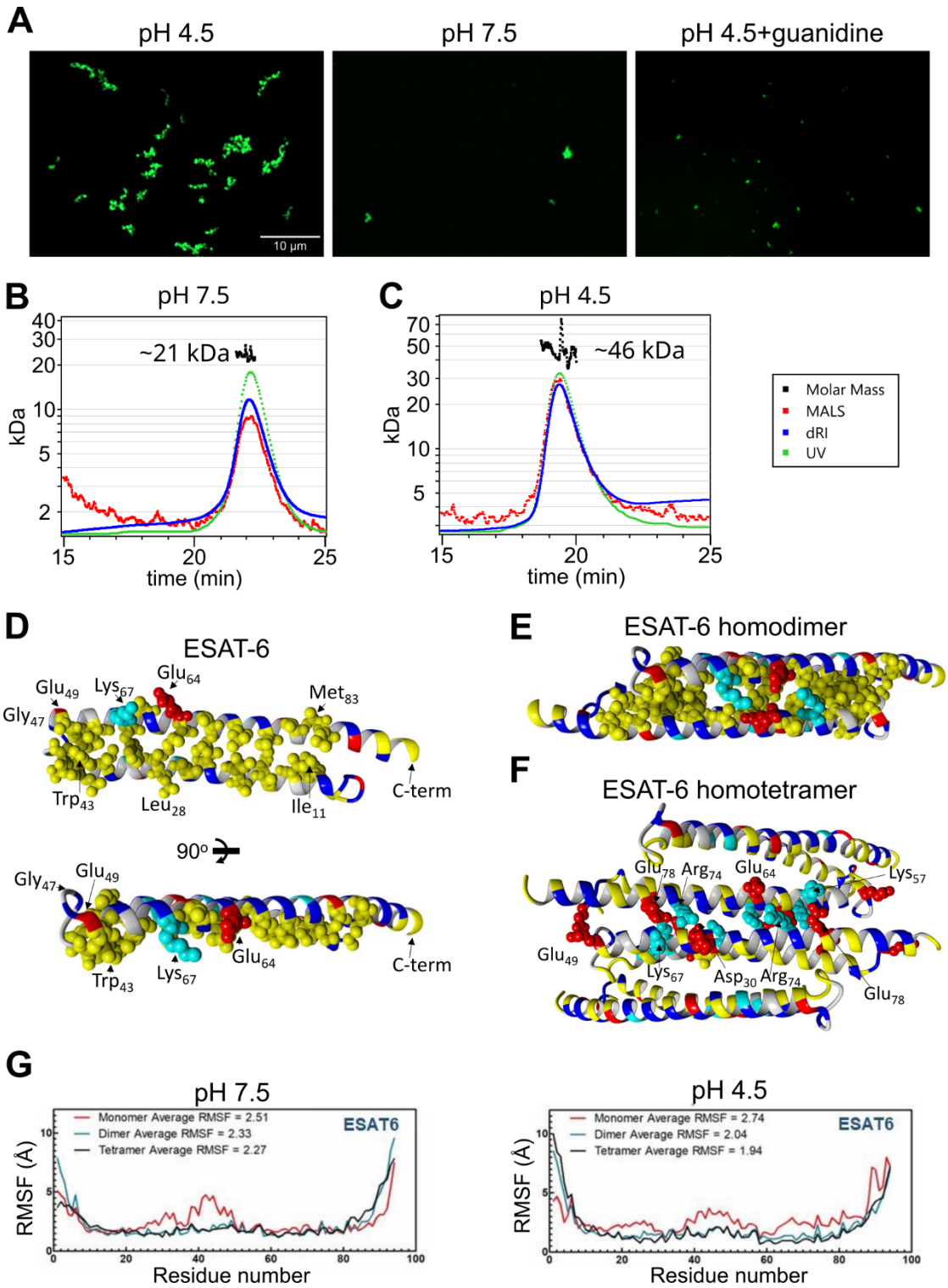


Figure 5: Stoichiometry of ESAT-6 self-interaction. (A) Fluorescence microscopy showing fluorescently labeled ESAT-6 complexes under different conditions: pH 4.5, pH 7.5, and pH 4.5 + 6M guanidine. The images shown are representative of 3 replicates. Size exclusion

732 chromatography followed by multi-angle light scattering (SEC-MALS) traces showing UV
733 absorbance, refractive index (dRI), and MALS data along with calculated molar mass over the
734 peak at pH 7.5 (B), and pH 4.5 (C). Data in (B-C) is representative of 3 replicates. (D-F) Modeling
735 of ESAT-6 in monomeric (D), homodimeric (E), and homotetrameric form (F). Hydrophobic
736 residues are in yellow, polar residues are in blue, basic residues are in cyan, and acidic residues
737 are in red. Key side chain residues are shown as spheres. (G) Root mean square fluctuation
738 (RMSF) values are shown per residue for ESAT-6 monomer, dimer, and trimer at pH 7.5 and 4.5.

739

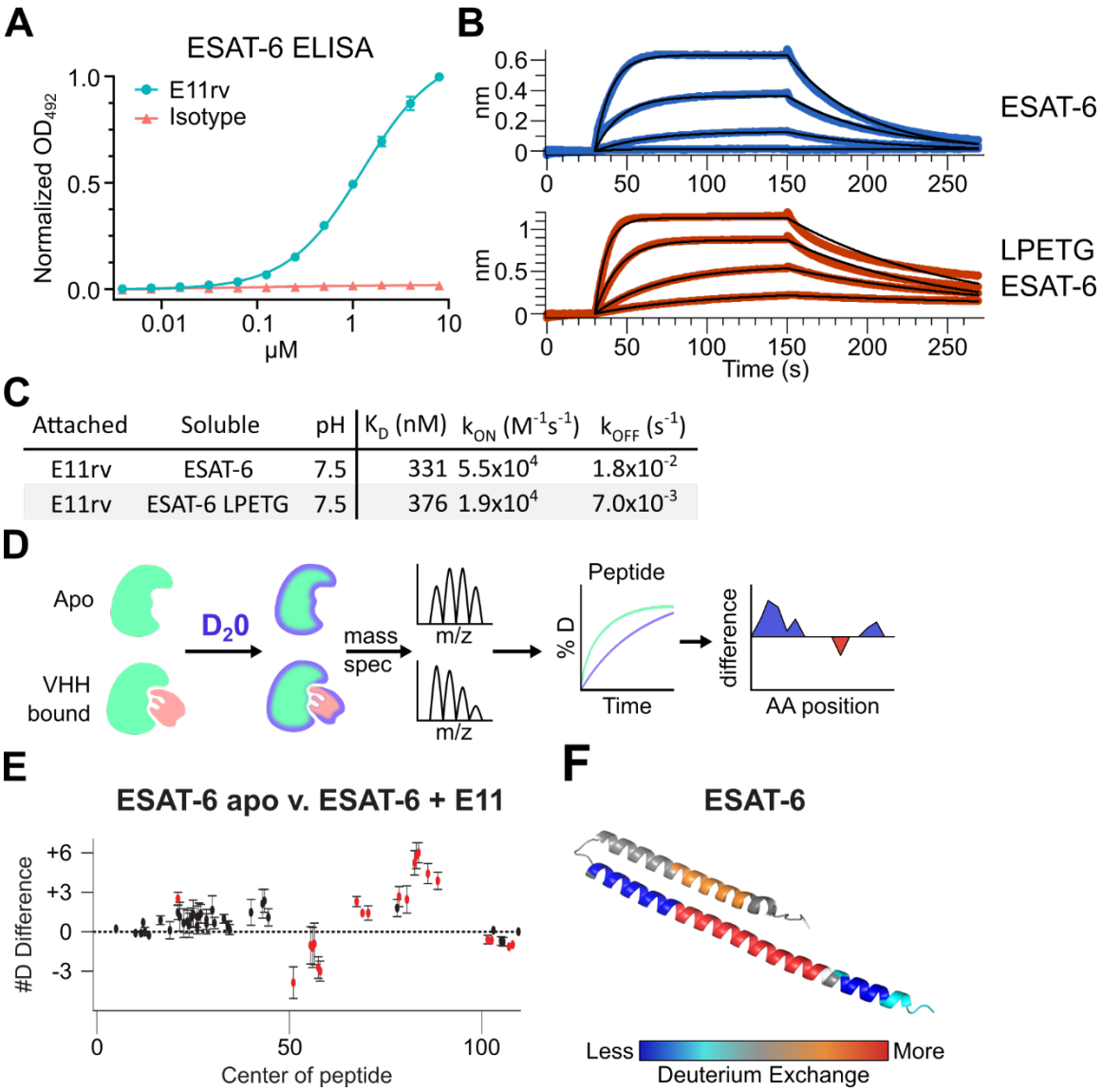


Figure 6: An ESAT-6-binding alpaca nanobody. (A) ELISA experiment on ESAT-6-coated plates showing nanobody E11rv and an irrelevant isotype control. E11rv displays an EC50 of 17.5 (95% CI 16.0-19.4) μg/mL. (B) BLI experiments with E11rv-coated biosensors tested against pMRLB.7 ESAT-6 (blue) or ESAT-6-LPETG (red) at 10, 3.3, 1, and 0.3 μM. (C) Summary of kinetic binding constants from (B). (D) schematic diagram of hydrogen-deuterium exchange (HDX) experiment showing apo ESAT-6 or E11rv-bound ESAT-6 incubated in D20, then subjected to digestion and mass spectrometry to measure the levels of deuterium incorporation at different times for different peptides, then mapping this to the protein sequence to identify areas with less

749 or greater deuterium exchange between the apo and bound conditions. (E) HDX data for ESAT-6
750 and E11rv showing reduced deuterium uptake around residue 50 and increased uptake around
751 residue 75. (F) HDX shifts mapped to the ESAT-6 structure (PDB: 3FAV).

752

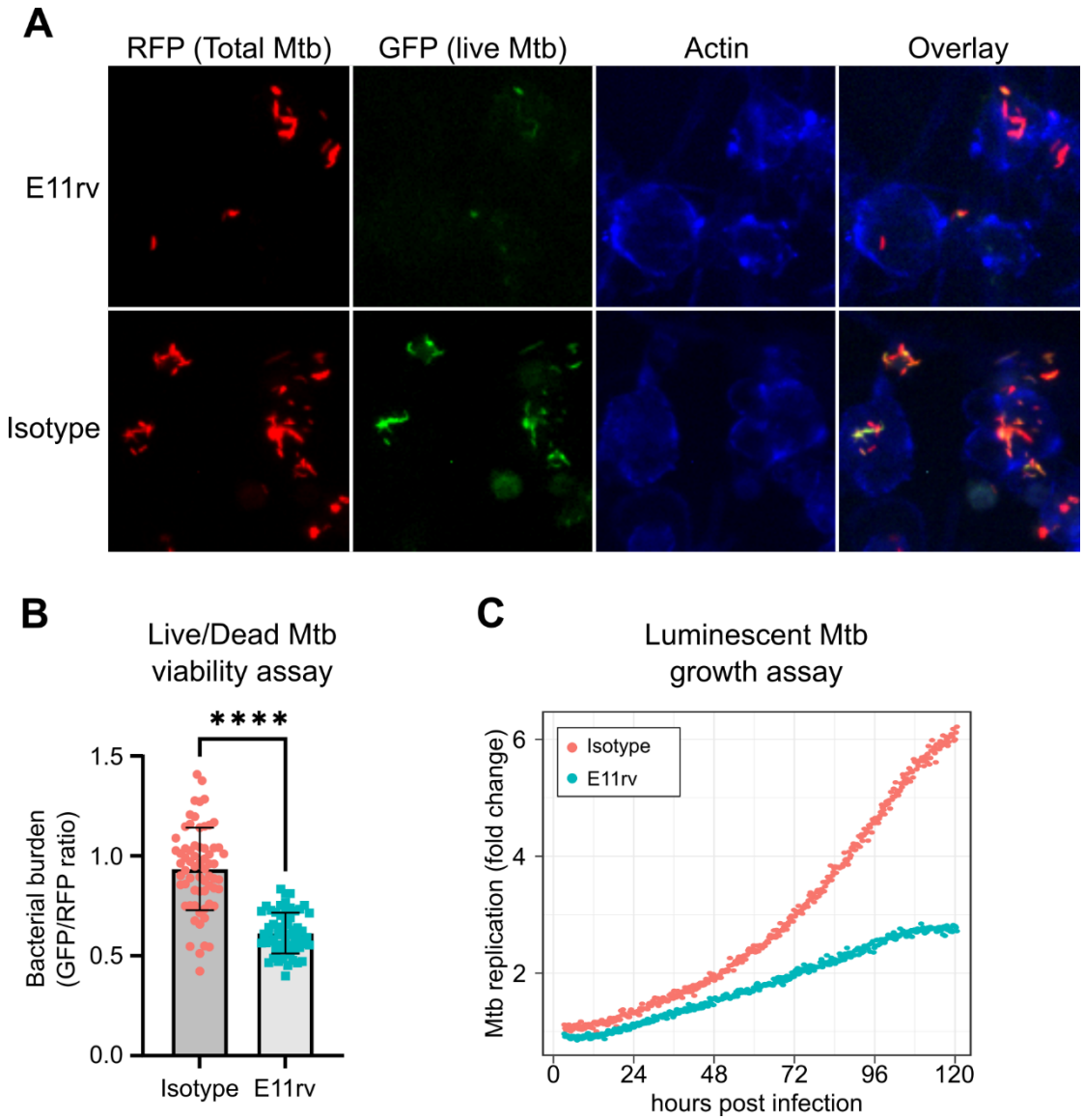


753

754 Figure 7: E11rv inhibits Mtb growth in cells. (A) representative fluorescence microscopy
755 images for E11rv and isotype treated cultures. Results include data from 3 replicates. (B) Cellular
756 assay testing the effect of infecting THP-1 cells with Live/Dead Mtb in the presence of E11rv for
757 3 days, treated with doxycycline for 24 hours to induce GFP expression by remaining
758 metabolically active Mtb. The GFP/RFP ratio was calculated for each Mtb spot identified by
759 fluorescence microscopy. Statistical significance was determined with a two-tailed unpaired t test.
760 * = 0.05, ** = 0.01, *** = 0.001, **** = 0.0001. (C) Luminescence growth assay of stably transfected
761 THP-1 cells expressing E11rv or isotype nanobody in their cytoplasm. Cells were infected with

762 luminescent Mtb and monitored by luminescence plate reader for 120 hours. Results are
763 representative of 6 replicates.

764

**A**

pMRLB.7 (ESAT-6)

```
                10        20        30        40        50        60
   1  CNNNNNNNCNNNNNANANTTTGTTTACTTTAAGAAGGAGATATACATATGACAGAGCAGC
  61  AGTGGAATTTCGCGGGTATCGAGGCCGCGGCAAGCGCAATCCAGGGAAATGTCACGTCCA
 121  TTCATTCCCTCCTTGACGAGGGGAAGCAGTCCCTGACCAAGCTCGCAGCGGCCTGGGGCG
 181  GTAGCGGTTCGGAGGCGTACCAGGGTGTCCAGCAAAAATGGGACGCCACGGCTACCGAGC
 241  TGAACAACGCGCTGCAGAACCTGGCGCGGACGATCAGCGAAGCCGGTCAGGCAATGGCTT
 301  CGACCGAAGGCAACGTCACTGGGATGTTCGCAGAGCTCATCAAGCTTATCGATACCGTCG
 361  ACCTCGAGCACCACCACCACCACCACTGAGATCCGGCTGCTAACAAAGCCCGAAAGGAAG
 421  CTGAGTTGGCTGCTGCCACCGCTGAGCAATAACTAGCATAACCCCTTGGGGCCTCTAAAC
 481  GGGTCTTGAGGGGTTTTTTGCTGAAAGGAGGAACTATATCCGGATTGGCGAATGGGACGC
 541  GCCCTGTAGCGGCGCATTAAGCGCGGCGGGTGTGGTGGTTACGCGCAGCGTGACCGCTAC
 601  ACTTGCCAGCGCCCTAGCGCCCGCTCCTTTCGCTTTCTTCCCTTCCTTTCTCGCCACGTT
 661  CGCCGGCTTTCCCCGTCAAGCTCTAAATCGGGGGCTCCCTTTAGGGTTCCGATTTAGTGC
 721  TTTACGGCACCTCGACCCCAAAAAACTTGATTANGGTGATGGTTCACGTAGTGGGCCATC
 781  GCCCTGATAGACGGTTTTTCGCCCTTTGACGTTGGAGTCCACGTTCTTTAATAGTGGACT
 841  CTTGTTCCAAACTGGNACAACACTCAACCCTATCTCGGTCTATTCTTTTGATTTATNANG
 901  NTTTTGCCGATTTCGGCCTATTGGNTAAAAATGAGCTGATTTAACAAAATTTAACGCGAA
 961  TTTANNNAATANTAACGCTTACATTTANNNGCACTTTTCGGGGAAATGTGCGNGACCCTN
1021  NTTGTTATTTTTCNAANACNTCANTATGNANCNCTCATGANANATANCNTGANAANGNTC
1081  ANAATNTNAAANNNNNNNATNANNATCANATTTCNNNNCNCCTATNCCNTTTNNNNGNNT
1141  TTNNNTNCNNNTTTNNNN
```

**B**

pMRLB.46 (CFP-10)

```
                10        20        30        40        50        60
   1  NNNNNNNNNNNNNNNNNNNNNNNNNTTTTGTTTAACTTTAAGAAGGAGATATACATATGGC
  61  AGAGATGAAGACCGATGCCGCTACCCTCGCGCAGGAGGCAGGTAATTTCGAGCGGATCTC
 121  CGGCGACCTGAAAACCCAGATCGACCAGGTGGAGTCGACGGCAGGTTCGTTGCAGGGCCA
 181  GTGGCGCGGCGCGGCGGGGACGGCCGCCCAGGCCGCGGTGGTGCGCTTCCAAGAAGCAGC
 241  CAATAAGCAGAAGCAGGAACTCGACGAGATCTCGACGAATATTCGTCAGGCCGGCGTCCA
 301  ATACTCGAGGGCCGACGAGGAGCAGCAGCAGGCGCTGTCCTCGCAAATGGGCTTCAAGCT
 361  TGCGGCCGCACTCGAGCACCACCACCACCACCACTGAGATCCGGCTGCTAACAAAGCCCG
 421  AAAGGAAGCTGAGTTGGCTGCTGCCACCGCTGAGCAATAACTAGCATAACCCCTTGGGGC
 481  CTCTAAACGGGTCTTGAGGGGTTTTTTGCTGAAAGGAGGAACTATATCCGGATTGGCGAA
 541  TGGGACGCGCCCTGTAGCGGCGCATTAAGCGCGGCGGGTGTGGTGGTTACGCGCAGCGTG
 601  ACCGCTACACTTGCCAGCGCCCTAGCGCCCGCTCCTTTCGCTTTCTTCCCTTCCTTTCTC
 661  GCCACGTTCGCCGGCTTTCCCCGTCAAGCTCTAAATCGGGGGCTCCCTTTAGGGTTCCGA
 721  TTTAGTGCTTTACGGCACCTCGACCCCAAAAAACTTGATTAGGGTGATGGTTCACGTAGT
 781  GGGNCATCGCCCTGATAGACGGNTTTTCGCCCTTTGACGTTGGAGTCCACGTTCTTTAAT
 841  AGTGGACTCTTGTTCCAANCTGGAACAACACTCAACCCTATCTCGGTCTATTCTTTTGAT
 901  TTATANGGATTTTGCCGATTTCGGCCTATTGGTTAAAAAATGAGCTGANTTAACNAAAAT
 961  TTAACGCGAATTTTNACNAAATATTAACGCTTNNAANTTANNNGGCACTTTTCGGGGAAN
1021  NGNNNNCGGAACCCCTATTTGGTNNTTTTTTCTAAATACATNCAANNNGNANCCGCTCNT
1081  NANANATAACCNNGANNNNGCTTCANAANNTTGAAAAGGAANANNNNNAGTATTCNANAN
1141  NTCNNGNNNCCCNNNNNNNN
```

765

766 Supplemental Figure S1: Sequencing of. (A) Sanger sequencing of pMRLB.7 with the ESAT-
767 6 open reading frame (ORF) highlighted grey. (B) Sanger sequencing of pMRLB.46 with the CFP-
768 10 ORF highlighted grey.

769

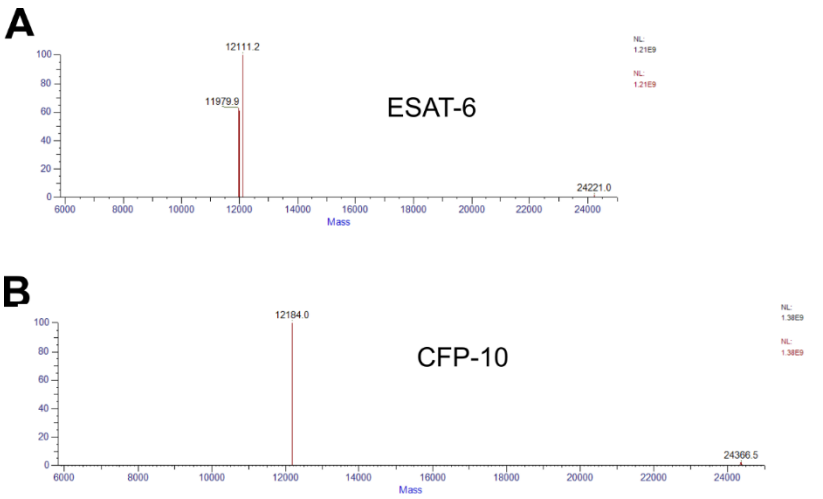


C

| | Computed mass (Da) | Measured mass (Da) | Fractional abundance (%) |
|---|---|---|---|
| ESAT-6 | 12109.2 | 12111.2 | 62 |
| ESAT-6ΔMet1 | 11978.0 | 11979.9 | 38 |
| CFP-10 | 12313.4 | ND | 0 |
| CFP-10ΔMet1 | 12182.2 | 12184.0 | 100 |

Supplemental Figure S2: Whole protein mass spectrometry (MS) of recombinant ESAT-6 and CFP-10. (A) Deconvoluted mass spectrum of recombinant ESAT-6 MS run. (B) Deconvoluted mass spectrum of recombinant CFP-10 MS run. (C) Computed mass of each protein compared with the measured masses. Fractional abundance combined the main peak with the harmonic artifact at twice the mass and gives an approximate relative proportion of each molecule in the sample. ESAT-6 is approximately 38% demethionylated while CFP-10 is fully demethionylated.

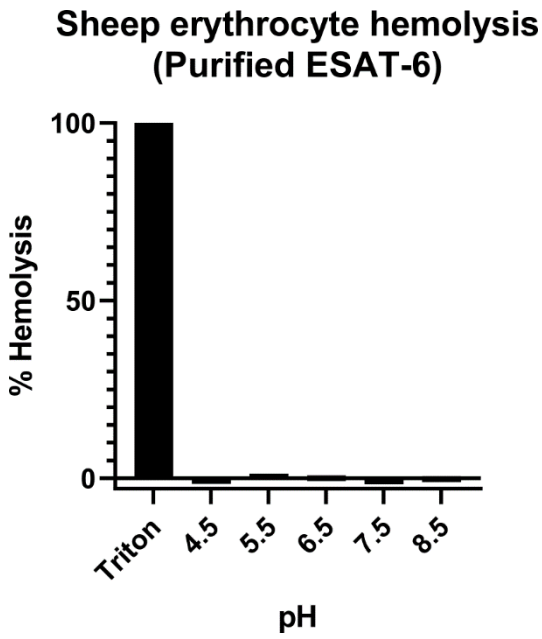


780

781 Supplemental Figure S3: Hemolysis by recombinant ESAT-6. (A) Sheep red blood cell
782 hemolysis assay carried out with purified ESAT-6 in citrate buffer at various pH values. Percent
783 hemolysis was calculated by subtracting buffer background and dividing by Triton-X100 detergent
784 lysed samples.

785

786

## References Cited:


Aguilera, J., Karki, C.B., Li, L., Reyes, S.V., Estevao, I., Grajeda, B.I., Zhang, Q., Arico, C.D., Ouellet, H., Sun, J., 2020. Nα-Acetylation of the virulence factor EsxA is required for mycobacterial cytosolic translocation and virulence. J. Biol. Chem. 295, 5785–5794. https://doi.org/10.1074/jbc.RA119.012497

Alfadhli, A., Romanaggi, C., Barklis, R.L., Merutka, I., Bates, T.A., Tafesse, F.G., Barklis, E., 2021. Capsid-specific nanobody effects on HIV-1 assembly and infectivity. Virology 562, 19–28. https://doi.org/10.1016/j.virol.2021.07.001

Andersen, P., Andersen, A.B., Sørensen, A.L., Nagai, S., 1995. Recall of long-lived immunity to Mycobacterium tuberculosis infection in mice. J Immunol 154, 3359–3372.

Andreu, N., Zelmer, A., Fletcher, T., Elkington, P.T., Ward, T.H., Ripoll, J., Parish, T., Bancroft, G.J., Schaible, U., Robertson, B.D., Wiles, S., 2010. Optimisation of Bioluminescent Reporters for Use with Mycobacteria. PLoS One 5, e10777. https://doi.org/10.1371/journal.pone.0010777

Augenstreich, J., Arbues, A., Simeone, R., Haanappel, E., Wegener, A., Sayes, F., Chevalier, F.L., Chalut, C., Malaga, W., Guilhot, C., Brosch, R., Astarie-Dequeker, C., 2017. ESX-1 and phthiocerol dimycocerosates of Mycobacterium tuberculosis act in concert to cause phagosomal rupture and host cell apoptosis. Cellular Microbiology 19, e12726. https://doi.org/10.1111/cmi.12726

Augenstreich, J., Haanappel, E., Sayes, F., Simeone, R., Guillet, V., Mazeres, S., Chalut, C., Mourey, L., Brosch, R., Guilhot, C., Astarie-Dequeker, C., 2020. Phthiocerol Dimycocerosates From Mycobacterium tuberculosis Increase the Membrane Activity of Bacterial Effectors and Host Receptors. Frontiers in Cellular and Infection Microbiology 10.

Bachran, C., Schröder, M., Conrad, L., Cragnolini, J.J., Tafesse, F.G., Helming, L., Ploegh, H.L., Swee, L.K., 2017. The activity of myeloid cell-specific VHH immunotoxins is target-, epitope-, subset- and organ dependent. Sci Rep 7, 17916. https://doi.org/10.1038/s41598-017-17948-0

Behura, A., Mishra, Abtar, Chugh, S., Mawatwal, S., Kumar, A., Manna, D., Mishra, Amit, Singh, R., Dhiman, R., 2019. ESAT-6 modulates Calcimycin-induced autophagy through microRNA-30a in mycobacteria infected macrophages. Journal of Infection 79, 139–152. https://doi.org/10.1016/j.jinf.2019.06.001

Bosserman, R.E., Nicholson, K.R., Champion, M.M., Champion, P.A., 2019. A New ESX-1 Substrate in Mycobacterium marinum That Is Required for Hemolysis but Not Host Cell Lysis. J Bacteriol 201. https://doi.org/10.1128/JB.00760-18

Canton, J., Khezri, R., Glogauer, M., Grinstein, S., 2014. Contrasting phagosome pH regulation and maturation in human M1 and M2 macrophages. Mol Biol Cell 25, 3330–3341. https://doi.org/10.1091/mbc.E14-05-0967

Carlsson, F., Joshi, S.A., Rangell, L., Brown, E.J., 2009. Polar Localization of Virulence-Related Esx-1 Secretion in Mycobacteria. PLOS Pathogens 5, e1000285. https://doi.org/10.1371/journal.ppat.1000285

Chen, J.M., Boy-Röttger, S., Dhar, N., Sweeney, N., Buxton, R.S., Pojer, F., Rosenkrands, I., Cole, S.T., 2012. EspD is critical for the virulence-mediating ESX-1 secretion system in Mycobacterium tuberculosis. J Bacteriol 194, 884–893. https://doi.org/10.1128/JB.06417-11

Chen, Y., Xiao, J., Li, Y., Xiao, Y., Xiong, Y., Liu, Y., Wang, S., Ji, P., Zhao, G., Shen, H., Lu, S., Fan, X., Wang, Y., 2019. Mycobacterial Lipoprotein Z Triggers Efficient Innate and Adaptive Immunity for Protection Against Mycobacterium tuberculosis Infection. Frontiers in Immunology 9.

Choi, H.-H., Shin, D.-M., Kang, G., Kim, K.-H., Park, J.B., Hur, G.M., Lee, H.-M., Lim, Y.-J., Park, J.-K., Jo, E.-K., Song, C.-H., 2010. Endoplasmic reticulum stress response is involved in Mycobacterium tuberculosis protein ESAT-6-mediated apoptosis. FEBS Letters 584, 2445–2454. https://doi.org/10.1016/j.febslet.2010.04.050

Clemmensen, H.S., Knudsen, N.P.H., Rasmussen, E.M., Winkler, J., Rosenkrands, I., Ahmad, A., Lillebaek, T., Sherman, D.R., Andersen, P.L., Aagaard, C., 2017. An attenuated Mycobacterium tuberculosis clinical strain with a defect in ESX-1 secretion induces minimal host immune responses and pathology. Scientific Reports 7, 46666. https://doi.org/10.1038/srep46666

Collars, O.A., Jones, B.S., Hu, D.D., Weaver, S.D., Champion, M.M., Champion, P.A., 2023. An N-acetyltransferase required for EsxA N-terminal protein acetylation and virulence in Mycobacterium marinum. bioRxiv 2023.03.14.532585. https://doi.org/10.1101/2023.03.14.532585

Conrad, W.H., Osman, M.M., Shanahan, J.K., Chu, F., Takaki, K.K., Cameron, J., Hopkinson-Woolley, D., Brosch, R., Ramakrishnan, L., 2017. Mycobacterial ESX-1 secretion system mediates host cell lysis through bacterium contact-dependent gross membrane disruptions. Proc Natl Acad Sci U S A 114, 1371–1376. https://doi.org/10.1073/pnas.1620133114

Cronin, R.M., Ferrell, M.J., Cahir, C.W., Champion, M.M., Champion, P.A., 2022. Proteo-genetic analysis reveals clear hierarchy of ESX-1 secretion in Mycobacterium marinum. Proc Natl Acad Sci U S A 119, e2123100119. https://doi.org/10.1073/pnas.2123100119

de Jonge, M.I., Pehau-Arnaudet, G., Fretz, M.M., Romain, F., Bottai, D., Brodin, P., Honoré, N., Marchal, G., Jiskoot, W., England, P., Cole, S.T., Brosch, R., 2007. ESAT-6 from Mycobacterium tuberculosis dissociates from its putative chaperone CFP-10 under acidic conditions and exhibits membrane-lysing activity. J Bacteriol 189, 6028–6034. https://doi.org/10.1128/JB.00469-07

De Leon, J., Jiang, G., Ma, Y., Rubin, E., Fortune, S., Sun, J., 2012. Mycobacterium tuberculosis ESAT-6 exhibits a unique membrane-interacting activity that is not found in its ortholog from non-pathogenic Mycobacterium smegmatis. J Biol Chem 287, 44184–44191. https://doi.org/10.1074/jbc.M112.420869

Dong, H., Jing, W., Runpeng, Z., Xuewei, X., Min, M., Ru, C., Yingru, X., Shengfa, N., Rongbo, Z., 2016. ESAT6 inhibits autophagy flux and promotes BCG proliferation through MTOR. Biochemical and Biophysical Research Communications 477, 195–201. https://doi.org/10.1016/j.bbrc.2016.06.042

Eitson, J.L., Medeiros, J.J., Hoover, A.R., Srivastava, S., Roybal, K.T., Aínsa, J.A., Hansen, E.J., Gumbo, T., van Oers, N.S.C., 2012. Mycobacterial Shuttle Vectors Designed for High-Level Protein Expression in Infected Macrophages. Appl Environ Microbiol 78, 6829–6837. https://doi.org/10.1128/AEM.01674-12

Fan, Y., Tan, K., Chhor, G., Butler, E.K., Jedrzejczak, R.P., Missiakas, D., Joachimiak, A., 2015. EsxB, a secreted protein from Bacillus anthracis forms two distinct helical bundles. Protein Sci 24, 1389–1400. https://doi.org/10.1002/pro.2715

Frei, J.C., Lai, J.R., 2016. Protein and Antibody Engineering by Phage Display, in: Methods in Enzymology. Elsevier, pp. 45–87. https://doi.org/10.1016/bs.mie.2016.05.005

Gallegos, A.M., Pamer, E.G., Glickman, M.S., 2008. Delayed protection by ESAT-6–specific effector CD4+ T cells after airborne M. tuberculosis infection. Journal of Experimental Medicine 205, 2359–2368. https://doi.org/10.1084/jem.20080353

García-Nafría, J., Watson, J.F., Greger, I.H., 2016. IVA cloning: A single-tube universal cloning system exploiting bacterial In Vivo Assembly. Sci Rep 6, 27459. https://doi.org/10.1038/srep27459

885 Gey van Pittius, N.C., Gamieldien, J., Hide, W., Brown, G.D., Siezen, R.J., Beyers, A.D., 2001.
886 The ESAT-6 gene cluster of Mycobacterium tuberculosis and other high G+C Gram-
887 positive bacteria. Genome Biol 2, research0044.1-research0044.18.
888 Giglione, C., Boularot, A., Meinnel, T., 2004. Protein N-terminal methionine excision. Cell Mol Life
889 Sci 61, 1455–1474. https://doi.org/10.1007/s00018-004-3466-8
890 Guimaraes, C.P., Witte, M.D., Theile, C.S., Bozkurt, G., Kundrat, L., Blom, A.E.M., Ploegh, H.L.,
891 2013. Site-specific C-terminal and internal loop labeling of proteins using sortase-
892 mediated reactions. Nat Protoc 8, 1787–1799. https://doi.org/10.1038/nprot.2013.101
893 Harris, N.J., Jenkins, M.L., Nam, S.-E., Rathinaswamy, M.K., Parson, M.A.H., Ranga-Prasad, H.,
894 Dalwadi, U., Moeller, B.E., Sheeky, E., Hansen, S.D., Yip, C.K., Burke, J.E., 2023.
895 Allosteric activation or inhibition of PI3Kγ mediated through conformational changes in the
896 p110γ helical domain. Elife 12, RP88058. https://doi.org/10.7554/eLife.88058
897 Harrison, D.E., Astle, C.M., Niazi, M.K.K., Major, S., Beamer, G.L., 2014. Genetically diverse mice
898 are novel and valuable models of age-associated susceptibility to Mycobacterium
899 tuberculosis. Immunity & Ageing 11, 24. https://doi.org/10.1186/s12979-014-0024-6
900 Hirel, P.H., Schmitter, M.J., Dessen, P., Fayat, G., Blanquet, S., 1989. Extent of N-terminal
901 methionine excision from Escherichia coli proteins is governed by the side-chain length of
902 the penultimate amino acid. Proceedings of the National Academy of Sciences 86, 8247–
903 8251. https://doi.org/10.1073/pnas.86.21.8247
904 Hoogenboom, H.R., Griffiths, A.D., Johnson, K.S., Chiswell, D.J., Hudson, P., Winter, G., 1991.
905 Multi-subunit proteins on the surface of filamentous phage: methodologies for displaying
906 antibody (Fab) heavy and light chains. Nucleic Acids Res 19, 4133–4137.
907 https://doi.org/10.1093/nar/19.15.4133
908 Houben, D., Demangel, C., van Ingen, J., Perez, J., Baldeon, L., Abdallah, A.M., Caleechurn, L.,
909 Bottai, D., van Zon, M., de Punder, K., van der Laan, T., Kant, A., Bossers-de Vries, R.,
910 Willemsen, P., Bitter, W., van Soolingen, D., Brosch, R., van der Wel, N., Peters, P.J.,
911 2012. ESX-1-mediated translocation to the cytosol controls virulence of mycobacteria. Cell
912 Microbiol 14, 1287–98. https://doi.org/10.1111/j.1462-5822.2012.01799.x
913 Houben, R.M.G.J., Dodd, P.J., 2016. The Global Burden of Latent Tuberculosis Infection: A Re-
914 estimation Using Mathematical Modelling. PLOS Medicine 13, e1002152.
915 https://doi.org/10.1371/journal.pmed.1002152
916 Jang, A.R., Choi, J.H., Shin, S.J., Park, J.H., 2018. Mycobacterium tuberculosis ESAT6 induces
917 IFN-beta gene expression in Macrophages via TLRs-mediated signaling. Cytokine 104,
918 104–109. https://doi.org/10.1016/j.cyto.2017.10.006
919 Karki, C., Xian, Y., Xie, Y., Sun, S., Lopez-Hernandez, A.E., Juarez, B., Wang, J., Sun, J., Li, L.,
920 2020. A computational model of ESAT-6 complex in membrane. J Theor Comput Chem
921 19, 2040002. https://doi.org/10.1142/s0219633620400027
922 Kinhikar, A.G., Verma, I., Chandra, D., Singh, K.K., Weldingh, K., Andersen, P., Hsu, T., Jacobs,
923 W.R., Laal, S., 2010. Potential role for ESAT6 in dissemination of M. tuberculosis via
924 human lung epithelial cells. Mol Microbiol 75, 92–106. https://doi.org/10.1111/j.1365-
925 2958.2009.06959.x
926 Koo, I.C., Wang, C., Raghavan, S., Morisaki, J.H., Cox, J.S., Brown, E.J., 2008. ESX-1-dependent
927 cytolysis in lysosome secretion and inflammasome activation during mycobacterial
928 infection. Cell Microbiol 10, 1866–1878. https://doi.org/10.1111/j.1462-5822.2008.01177.x
929 Koyuncu, D., Niazi, M.K.K., Tavolara, T., Abeijon, C., Ginese, M.L., Liao, Y., Mark, C., Specht, A.,
930 Gower, A.C., Restrepo, B.I., Gatti, D.M., Kramnik, I., Gurcan, M., Yener, B., Beamer, G.,
931 2021. CXCL1: A new diagnostic biomarker for human tuberculosis discovered using
932 Diversity Outbred mice. PLOS Pathogens 17, e1009773.
933 https://doi.org/10.1371/journal.ppat.1009773
934 Kumar, P., Agarwal, R., Siddiqui, I., Vora, H., Das, G., Sharma, P., 2012. ESAT6 differentially
935 inhibits IFN-γ-inducible class II transactivator isoforms in both a TLR2-dependent and -

independent manner. Immunology & Cell Biology 90, 411–420. https://doi.org/10.1038/icb.2011.54

Leddy, O., White, F.M., Bryson, B.D., 2023. Immunopeptidomics reveals determinants of Mycobacterium tuberculosis antigen presentation on MHC class I. eLife 12, e84070. https://doi.org/10.7554/eLife.84070

Lienard, J., Nobs, E., Lovins, V., Movert, E., Valfridsson, C., Carlsson, F., 2020. The Mycobacterium marinum ESX-1 system mediates phagosomal permeabilization and type I interferon production via separable mechanisms. Proc Natl Acad Sci U S A 117, 1160–1166. https://doi.org/10.1073/pnas.1911646117

Lightbody, K.L., Ilghari, D., Waters, L.C., Carey, G., Bailey, M.A., Williamson, R.A., Renshaw, P.S., Carr, M.D., 2008. Molecular features governing the stability and specificity of functional complex formation by Mycobacterium tuberculosis CFP-10/ESAT-6 family proteins. J Biol Chem 283, 17681–17690. https://doi.org/10.1074/jbc.M800123200

Lim, Y.-J., Yi, M.-H., Choi, J.-A., Lee, J., Han, J.-Y., Jo, S.-H., Oh, S.-M., Cho, H.J., Kim, D.W., Kang, M.-W., Song, C.-H., 2016. Roles of endoplasmic reticulum stress-mediated apoptosis in M1-polarized macrophages during mycobacterial infections. Sci Rep 6, 37211. https://doi.org/10.1038/srep37211

López-Jiménez, A.T., Cardenal-Muñoz, E., Leuba, F., Gerstenmaier, L., Barisch, C., Hagedorn, M., King, J.S., Soldati, T., 2018. The ESCRT and autophagy machineries cooperate to repair ESX-1-dependent damage at the Mycobacterium-containing vacuole but have opposite impact on containing the infection. PLOS Pathogens 14, e1007501. https://doi.org/10.1371/journal.ppat.1007501

Maass, D.R., Sepulveda, J., Pernthaner, A., Shoemaker, C.B., 2007. Alpaca (Lama pacos) as a convenient source of recombinant camelid heavy chain antibodies (VHHs). J Immunol Methods 324, 13–25. https://doi.org/10.1016/j.jim.2007.04.008

Martin, C.J., Booty, M.G., Rosebrock, T.R., Nunes-Alves, C., Desjardins, D.M., Keren, I., Fortune, S.M., Remold, H.G., Behar, S.M., 2012. Efferocytosis is an innate antibacterial mechanism. Cell Host Microbe 12, 289–300. https://doi.org/10.1016/j.chom.2012.06.010

Masson, G.R., Burke, J.E., Ahn, N.G., Anand, G.S., Borchers, C., Brier, S., Bou-Assaf, G.M., Engen, J.R., Englander, S.W., Faber, J., Garlish, R., Griffin, P.R., Gross, M.L., Guttman, M., Hamuro, Y., Heck, A.J.R., Houde, D., Iacob, R.E., Jørgensen, T.J.D., Kaltashov, I.A., Klinman, J.P., Konermann, L., Man, P., Mayne, L., Pascal, B.D., Reichmann, D., Skehel, M., Snijder, J., Strutzenberg, T.S., Underbakke, E.S., Wagner, C., Wales, T.E., Walters, B.T., Weis, D.D., Wilson, D.J., Wintrode, P.L., Zhang, Z., Zheng, J., Schriemer, D.C., Rand, K.D., 2019. Recommendations for performing, interpreting and reporting hydrogen deuterium exchange mass spectrometry (HDX-MS) experiments. Nat Methods 16, 595–602. https://doi.org/10.1038/s41592-019-0459-y

Mba Medie, F., Champion, M.M., Williams, E.A., Champion, P.A.D., 2014. Homeostasis of N-α-Terminal Acetylation of EsxA Correlates with Virulence in Mycobacterium marinum. Infect Immun 82, 4572–4586. https://doi.org/10.1128/IAI.02153-14

McIlvaine, T.C., 1921. A BUFFER SOLUTION FOR COLORIMETRIC COMPARISON. Journal of Biological Chemistry 49, 183–186. https://doi.org/10.1016/S0021-9258(18)86000-8

Meerbrey, K.L., Hu, G., Kessler, J.D., Roarty, K., Li, M.Z., Fang, J.E., Herschkowitz, J.I., Burrows, A.E., Ciccia, A., Sun, T., Schmitt, E.M., Bernardi, R.J., Fu, X., Bland, C.S., Cooper, T.A., Schiff, R., Rosen, J.M., Westbrook, T.F., Elledge, S.J., 2011. The pINDUCER lentiviral toolkit for inducible RNA interference in vitro and in vivo. Proc Natl Acad Sci U S A 108, 3665–3670. https://doi.org/10.1073/pnas.1019736108

Mukherjee, P., Dutta, M., Datta, P., Dasgupta, A., Pradhan, R., Pradhan, M., Kundu, M., Basu, J., Chakrabarti, P., 2007. The RD1-encoded antigen Rv3872 of Mycobacterium tuberculosis as a potential candidate for serodiagnosis of tuberculosis. Clinical Microbiology and Infection 13, 146–152. https://doi.org/10.1111/j.1469-0691.2006.01660.x

Niazi, M.K.K., Dhulekar, N., Schmidt, D., Major, S., Cooper, R., Abeijon, C., Gatti, D.M., Kramnik, I., Yener, B., Gurcan, M., Beamer, G., 2015. Lung necrosis and neutrophils reflect common pathways of susceptibility to Mycobacterium tuberculosis in genetically diverse, immune-competent mice. Dis Model Mech 8, 1141–1153. https://doi.org/10.1242/dmm.020867

Niekamp, P., Guzman, G., Leier, H.C., Rashidfarrokhi, A., Richina, V., Pott, F., Barisch, C., Holthuis, J.C.M., Tafesse, F.G., 2021. Sphingomyelin Biosynthesis Is Essential for Phagocytic Signaling during Mycobacterium tuberculosis Host Cell Entry. mBio 12, e03141-20. https://doi.org/10.1128/mBio.03141-20

Okkels, L.M., Müller, E.-C., Schmid, M., Rosenkrands, I., Kaufmann, S.H.E., Andersen, P., Jungblut, P.R., 2004. CFP10 discriminates between nonacetylated and acetylated ESAT-6 of Mycobacterium tuberculosis by differential interaction. PROTEOMICS 4, 2954–2960. https://doi.org/10.1002/pmic.200400906

Osman, M.M., Shanahan, J.K., Chu, F., Takaki, K.K., Pinckert, M.L., Pagán, A.J., Brosch, R., Conrad, W.H., Ramakrishnan, L., 2022. The C terminus of the mycobacterium ESX-1 secretion system substrate ESAT-6 is required for phagosomal membrane damage and virulence. Proc Natl Acad Sci U S A 119, e2122161119. https://doi.org/10.1073/pnas.2122161119

Pathak, S.K., Basu, S., Basu, K.K., Banerjee, A., Pathak, S., Bhattacharyya, A., Kaisho, T., Kundu, M., Basu, J., 2007. Direct extracellular interaction between the early secreted antigen ESAT-6 of Mycobacterium tuberculosis and TLR2 inhibits TLR signaling in macrophages. Nat Immunol 8, 610–618. https://doi.org/10.1038/ni1468

Peng, H., Wang, X., Barnes, P.F., Tang, H., Townsend, J.C., Samten, B., 2011. The Mycobacterium tuberculosis Early Secreted Antigenic Target of 6 kDa Inhibits T Cell Interferon-γ Production through the p38 Mitogen-activated Protein Kinase Pathway. J Biol Chem 286, 24508–24518. https://doi.org/10.1074/jbc.M111.234062

Perez-Riverol, Y., Bai, J., Bandla, C., García-Seisdedos, D., Hewapathirana, S., Kamatchinathan, S., Kundu, D.J., Prakash, A., Frericks-Zipper, A., Eisenacher, M., Walzer, M., Wang, S., Brazma, A., Vizcaíno, J.A., 2022. The PRIDE database resources in 2022: a hub for mass spectrometry-based proteomics evidences. Nucleic Acids Res 50, D543–D552. https://doi.org/10.1093/nar/gkab1038

Popp, M.W., Antos, J.M., Ploegh, H.L., 2009. Site-specific protein labeling via sortase-mediated transpeptidation. Curr Protoc Protein Sci Chapter 15, Unit 15 3. https://doi.org/10.1002/0471140864.ps1503s56

Poulsen, C., Panjikar, S., Holton, S.J., Wilmanns, M., Song, Y.-H., 2014. WXG100 Protein Superfamily Consists of Three Subfamilies and Exhibits an α-Helical C-Terminal Conserved Residue Pattern. PLOS ONE 9, e89313. https://doi.org/10.1371/journal.pone.0089313

Rathinaswamy, M.K., Fleming, K.D., Dalwadi, U., Pardon, E., Harris, N.J., Yip, C.K., Steyaert, J., Burke, J.E., 2021. HDX-MS-optimized approach to characterize nanobodies as tools for biochemical and structural studies of class IB phosphoinositide 3-kinases. Structure 29, 1371-1381.e6. https://doi.org/10.1016/j.str.2021.07.002

Refai, A., Haoues, M., Othman, H., Barbouche, M.R., Moua, P., Bondon, A., Mouret, L., Srairi-Abid, N., Essafi, M., 2015. Two distinct conformational states of Mycobacterium tuberculosis virulent factor early secreted antigenic target 6 kDa are behind the discrepancy around its biological functions. The FEBS Journal 282, 4114–4129. https://doi.org/10.1111/febs.13408

Renshaw, P.S., Lightbody, K.L., Veverka, V., Muskett, F.W., Kelly, G., Frenkiel, T.A., Gordon, S.V., Hewinson, R.G., Burke, B., Norman, J., Williamson, R.A., Carr, M.D., 2005. Structure and function of the complex formed by the tuberculosis virulence factors CFP-10 and ESAT-6. The EMBO Journal 24, 2491–2498. https://doi.org/10.1038/sj.emboj.7600732

1037 Renshaw, P.S., Panagiotidou, P., Whelan, A., Gordon, S.V., Hewinson, R.G., Williamson, R.A.,
1038 Carr, M.D., 2002. Conclusive Evidence That the Major T-cell Antigens of
1039 theMycobacterium tuberculosis Complex ESAT-6 and CFP-10 Form a Tight, 1:1 Complex
1040 and Characterization of the Structural Properties of ESAT-6, CFP-10, and the ESAT-
1041 6·CFP-10 Complex: IMPLICATIONS FOR PATHOGENESIS AND VIRULENCE *. Journal
1042 of Biological Chemistry 277, 21598–21603. https://doi.org/10.1074/jbc.M201625200
1043 Romagnoli, A., Etna, M.P., Giacomini, E., Pardini, M., Remoli, M.E., Corazzari, M., Falasca, L.,
1044 Goletti, D., Gafa, V., Simeone, R., Delogu, G., Piacentini, M., Brosch, R., Fimia, G.M.,
1045 Coccia, E.M., 2012. ESX-1 dependent impairment of autophagic flux by Mycobacterium
1046 tuberculosis in human dendritic cells. Autophagy 8, 1357–1370.
1047 https://doi.org/10.4161/auto.20881
1048 Sanchez, K.G., Ferrell, M.J., Chirakos, A.E., Nicholson, K.R., Abramovitch, R.B., Champion,
1049 M.M., Champion, P.A., 2020. EspM Is a Conserved Transcription Factor That Regulates
1050 Gene Expression in Response to the ESX-1 System. mBio 11.
1051 https://doi.org/10.1128/mBio.02807-19
1052 Santucci, P., Aylan, B., Botella, L., Bernard, E.M., Bussi, C., Pellegrino, E., Athanasiadi, N.,
1053 Gutierrez, M.G., 2022. Visualizing Pyrazinamide Action by Live Single-Cell Imaging of
1054 Phagosome Acidification and Mycobacterium tuberculosis pH Homeostasis. mBio 13,
1055 e00117-22. https://doi.org/10.1128/mbio.00117-22
1056 Schnettger, L., Rodgers, A., Repnik, U., Lai, R.P., Pei, G., Verdoes, M., Wilkinson, R.J., Young,
1057 D.B., Gutierrez, M.G., 2017. A Rab20-Dependent Membrane Trafficking Pathway Controls
1058 M. tuberculosis Replication by Regulating Phagosome Spaciousness and Integrity. Cell
1059 Host & Microbe 21, 619-628.e5. https://doi.org/10.1016/j.chom.2017.04.004
1060 Smith, J., Manoranjan, J., Pan, M., Bohsali, A., Xu, J., Liu, J., McDonald, K.L., Szyk, A., LaRonde-
1061 LeBlanc, N., Gao, L.-Y., 2008. Evidence for Pore Formation in Host Cell Membranes by
1062 ESX-1-Secreted ESAT-6 and Its Role in Mycobacterium marinum Escape from the
1063 Vacuole. Infect Immun 76, 5478–5487. https://doi.org/10.1128/IAI.00614-08
1064 Sørensen, A.L., Nagai, S., Houen, G., Andersen, P., Andersen, A.B., 1995. Purification and
1065 characterization of a low-molecular-mass T-cell antigen secreted by Mycobacterium
1066 tuberculosis. Infect Immun 63, 1710–1717. https://doi.org/10.1128/iai.63.5.1710-
1067 1717.1995
1068 Sreejit, G., Ahmed, A., Parveen, N., Jha, V., Valluri, V.L., Ghosh, S., Mukhopadhyay, S., 2014.
1069 The ESAT-6 Protein of Mycobacterium tuberculosis Interacts with Beta-2-Microglobulin
1070 (β2M) Affecting Antigen Presentation Function of Macrophage. PLOS Pathogens 10,
1071 e1004446. https://doi.org/10.1371/journal.ppat.1004446
1072 Stariha, J.T.B., Hoffmann, R.M., Hamelin, D.J., Burke, J.E., 2021. Probing Protein-Membrane
1073 Interactions and Dynamics Using Hydrogen-Deuterium Exchange Mass Spectrometry
1074 (HDX-MS). Methods Mol Biol 2263, 465–485. https://doi.org/10.1007/978-1-0716-1197-
1075 5_22
1076 Stavri, H., Bucurenci, N., Ulea, I., Costache, A., Popa, L., Popa, M.I., 2012. Use of recombinant
1077 purified protein derivative (PPD) antigens as specific skin test for tuberculosis. Indian
1078 Journal of Medical Research 136, 799.
1079 Stirling, D.R., Swain-Bowden, M.J., Lucas, A.M., Carpenter, A.E., Cimini, B.A., Goodman, A.,
1080 2021. CellProfiler 4: improvements in speed, utility and usability. BMC Bioinformatics 22,
1081 433. https://doi.org/10.1186/s12859-021-04344-9
1082 Tak, U., Dokland, T., Niederweis, M., 2021. Pore-forming Esx proteins mediate toxin secretion by
1083 Mycobacterium tuberculosis. Nat Commun 12. https://doi.org/10.1038/s41467-020-
1084 20533-1
1085 Vesosky, B., Rottinghaus, E.K., Stromberg, P., Turner, J., Beamer, G., 2010. CCL5 participates in
1086 early protection against Mycobacterium tuberculosis. Journal of Leukocyte Biology 87,
1087 1153–1165. https://doi.org/10.1189/jlb.1109742

1088 Weinstein, J.B., Bates, T.A., Leier, H.C., McBride, S.K., Barklis, E., Tafesse, F.G., 2022. A potent
1089 alpaca-derived nanobody that neutralizes SARS-CoV-2 variants. iScience 25, 103960.
1090 https://doi.org/10.1016/j.isci.2022.103960
1091 Woolhiser, L., Tamayo, M.H., Wang, B., Gruppo, V., Belisle, J.T., Lenaerts, A.J., Basaraba, R.J.,
1092 Orme, I.M., 2007. In Vivo Adaptation of the Wayne Model of Latent Tuberculosis. Infection
1093 and Immunity 75, 2621–2625. https://doi.org/10.1128/iai.00918-06
1094 World Health Organization, 2022. Global tuberculosis report 2022. World Health Organization,
1095 Geneva.
1096 Xiao, Y., Sha, W., Tian, Z., Chen, Y., Ji, P., Sun, Q., Wang, H., Wang, S., Fang, Y., Wen, H.-L.,
1097 Zhao, H., Lu, J., Xiao, H., Fan, X., Shen, H., Wang, Y., 2016. Adenylate kinase: a novel
1098 antigen for immunodiagnosis and subunit vaccine against tuberculosis. J Mol Med 94,
1099 823–834. https://doi.org/10.1007/s00109-016-1392-5
1100 Yabaji, S.M., Dhamija, E., Mishra, A.K., Srivastava, K.K., 2020. ESAT-6 regulates autophagous
1101 response through SOD-2 and as a result induces intracellular survival of Mycobacterium
1102 bovis BCG. Biochimica et Biophysica Acta (BBA) - Proteins and Proteomics 1868, 140470.
1103 https://doi.org/10.1016/j.bbapap.2020.140470
1104 Yang, C.-S., Lee, J.-S., Lee, H.-M., Sun Shim, T., Woong Son, J., Jung, S.-S., Kim, J.-S., Song,
1105 C.-H., Kim, H.-J., Jo, E.-K., 2008. Differential cytokine levels and immunoreactivities
1106 against Mycobacterium tuberculosis antigens between tuberculous and malignant
1107 effusions. Respiratory Medicine 102, 280–286.
1108 https://doi.org/10.1016/j.rmed.2007.08.016
1109 Yang, S., Li, F., Jia, S., Zhang, K., Jiang, W., Shang, Y., Chang, K., Deng, S., Chen, M., 2015.
1110 Early secreted antigen ESAT-6 of Mycobacterium Tuberculosis promotes apoptosis of
1111 macrophages via targeting the microRNA155-SOCS1 interaction. Cell. Physiol. Biochem.
1112 35, 1276–1288. https://doi.org/10.1159/000373950
1113